Supplementary Information

Liquid–Liquid Interfacial Approach for the Facile Synthesis of Tp-NBD COFs for Efficient Photocatalytic Hydrogen Production

Syeda Andleeb Zahra Naqvi, [ab] Ateeq Ur Rehman Baloch, [ab] Umm Y Umna, [ab] Kamran Muzaffar, [ab] Tayyab Sohail Aslam, [ab] Jinsong Chen*[abc] Yaobing Wang*[abc]

[a] CAS Key Laboratory of Design and Assembly of Functional Nanostructures, and Fujian Provincial Key Laboratory of Nanomaterials, State Key Laboratory of Structural Chemistry, Fujian Institute of Research on the Structure of Matter, Chinese Academy of Sciences, Fuzhou 350002, Fujian, P. R. China.

[b] University of Chinese Academy of Sciences, Beijing 100049, P. R. China

[c] Fujian Science and Technology Innovation Laboratory for Optoelectronic Information of China, Fuzhou 350108, Fujian, P. R. China

Experimental Procedures

Materials and Methods

Liquid-Liquid Interfacial Synthesis Method

According to the reported procedure, [1] nM/Tp-NBD COFs were prepared following a liquid-liquid interfacial method with slight changes by taking equimolar amounts of aldehyde (Tp) and amine (NBD) monomers. In a 250 mL beaker, 0.1 mmol (21.04 mg) of Tp was dissolved in 40 mL of dichloromethane to form the aldehyde solution; then, 3, 6, 9, 12, 15 and 17M acetic acid solution (prepared in 20 mL DI water) was added slowly until the surface of the aldehyde solution was covered entirely (solution A). Later, 0.1 mmol of NBD (51.86 mg) was dissolved in 20 mL DMF to get an Amine solution (solution B). Next, solution B was added dropwise to the interface of solution A. After some time, the product was filtered and washed thoroughly with DCM, ethanol, acetone, and DMF, dried in a vacuum oven at 60 °C overnight (62 mg, 84% yield), and stored in a glass container for further investigation.

Solvothermal Synthesis Method

In a 10 mL Pyrex tube, equimolar amounts (0.1 mmol) of Tp (*1,3,5-triformylphloroglucinol*) and NBD (*N4, N4-bis(4'-amino-[1,1'-biphenyl]-4-yl)-[1,1'-biphenyl]-4,4'-diamine*) were dispersed in a mixture of mesitylene and 1,4-Dioxane (2/2 mL, v/v), followed by sonication for 20 minutes to obtain a homogeneous suspension. Subsequently, glacial acetic acid (0.5 mL, 12 M) was added, and after three freeze-pump-thaw cycles, the glass ampoule was vacuum-sealed and allowed to react at 120°C for 3 days. [2] The precipitates collected were filtered and washed with ethanol, anhydrous N, N-dimethylformamide, and acetone. The resultant product was dried overnight under a vacuum at 60°C and stored in a glass container for further evaluation.

Characterizations

The powder X-ray diffraction (PXRD) spectra were recorded on Rigaku Miniflex 600, with Cu Kα radiation in the scanning range of 2.5 to 40 ° at the rate of 5 degrees per minute. N_2 adsorption-desorption isotherm was measured with an ASAP 2020M automatic microporous analyzer (Micromeritics). ^{13}C cross-polarization/magic angle spinning solid-state nuclear magnetic resonance (CP/MAS-ssNMR) experiments were performed on a Bruker AVANCEIIIHD600WB spectrometer. Fourier-transform infrared (FT-IR) spectra were recorded in a Thermo Nicolet IS5 FT-IR (ATR) spectrometer. SEM measurements were performed with SU8010. The energy-dispersive X-ray spectroscopy (EDX) was conducted in a FEI Tecnai-F20 microscope. High-resolution transmission electron microscopy (HR-TEM) images were obtained using a JEOL 2100F Microscope. X-ray photoelectron spectroscopy (XPS) was recorded using an Escalab 250Xi instrument (Thermo Scientific). UV-vis diffuse reflectance spectra (UV-vis DRS) were recorded using a Lambda950 spectrophotometer with Barium Sulfate as a reference.

Photoelectrochemical Measurements

Mott-Schottky (MS), Photocurrent Response (PR), and Electrochemical Impedance (EIS) measurements were performed using a CHI workstation (CHI660E) in a three-electrode system, where COF-coated Florine-doped Tin Oxide (FTO) glass acted as a working electrode, a Pt electrode was used as a counter electrode, and an Ag/AgCl electrode acted as a standard. 0.5 M Na_2SO_4 solution was used as an electrolyte. FTO glass (1x2 cm^2) was cleaned by sonication in toluene, acetone, and ethanol for 30 minutes each. 5 mg of COF was dispersed via sonication in 1 mL of ethanol, followed by adding 50 µL of 5wt% Nafion to get a slurry. This slurry was thinly coated on the active side of the FTO glass to record the desired measurements. For Mott-Schottky measurements, varying frequencies (1500, 2000, 2500 Hz) were used at 10 mV amplitude. [3] The applied potentials (V vs. Ag/AgCl) were converted to NHE potentials using the following equation:

$$E_{NHE} = E_{Ag/AgCl} + E^{\theta}_{Ag/AgCl}\left(E^{\theta}_{Ag/AgCl}\right) = 0.197V$$

A 300 W Xe light source (PLSSXE300C, Perfectlight) was used for photocurrent measurements.

Evaluation of Photocatalytic HER

3 mg of a COF sample were dispersed via ultrasonication for 30 minutes in an aqueous solution of 0.05 M ascorbic acid (100 mL) and 2 wt. % $H_2PtCl_6.6H_2O$ (0.01 M aqueous solution) was used as a source of Pt cocatalyst. The reaction system was irradiated with a 300 W Xe lamp (PLSSXE300C, Perfectlight) using cut-on filters (AM 1.5 G) with stirring. The amount of hydrogen was measured with Labsolar-6A (Perfectlight), equipped with an online gas chromatography (GC, 7990, TCD detector, N_2 carrier). Different control experiments, including cyclic stability tests, were carried out in the same system. The reaction system was evacuated for 15-20 min between each cycle.

Apparent Quantum Yield (AQY) Measurement

The apparent quantum yield (AQY) for photocatalytic H_2 evolution was measured using a 300 W Xe lamp (PLS-SXE300C, Perfectlight) with different band-pass filters of 400, 450, 500, 500, 500, 550, and 600 nm. The intensities were 88, 163.5, 139.5, 209.7, and 227.3 W m^{-2}, respectively. The irradiation area was 7 cm^2. Depending on the amount of hydrogen produced by the photocatalytic reaction in one hour, the AQY were calculated using equations (1) and (2) below:

$$AQY\ (\%) = \frac{2\ x\ Number\ of\ H_2\ Molecules\ evolved}{Number\ of\ incident\ photons}\ x\ 100 \qquad (1)$$

$$AQY\ (\%) = \frac{2\ x\ NH_2\ x\ N_A\ x\ h\ x\ c}{S\ x\ P\ x\ t\ x\ \lambda} x\ 100 \qquad (2)$$

Where 2 is the number of electrons required for H_2 generation, NH_2 is the number of H_2 molecules (mol). NA is Avogadro's number (6.022 x 10^{23} mol^{-1}), c is the speed of light (3.0 x 10^8 ms^{-1}), *h* is the Planck's

constant (6.626×10^{-34} Js), S is the irradiation area (cm^2), P is the intensity of irradiation light ($W\ m^{-2}$), t is the irradiation time (s), and λ is the wavelength of the monochromatic light (m). [4, 5]

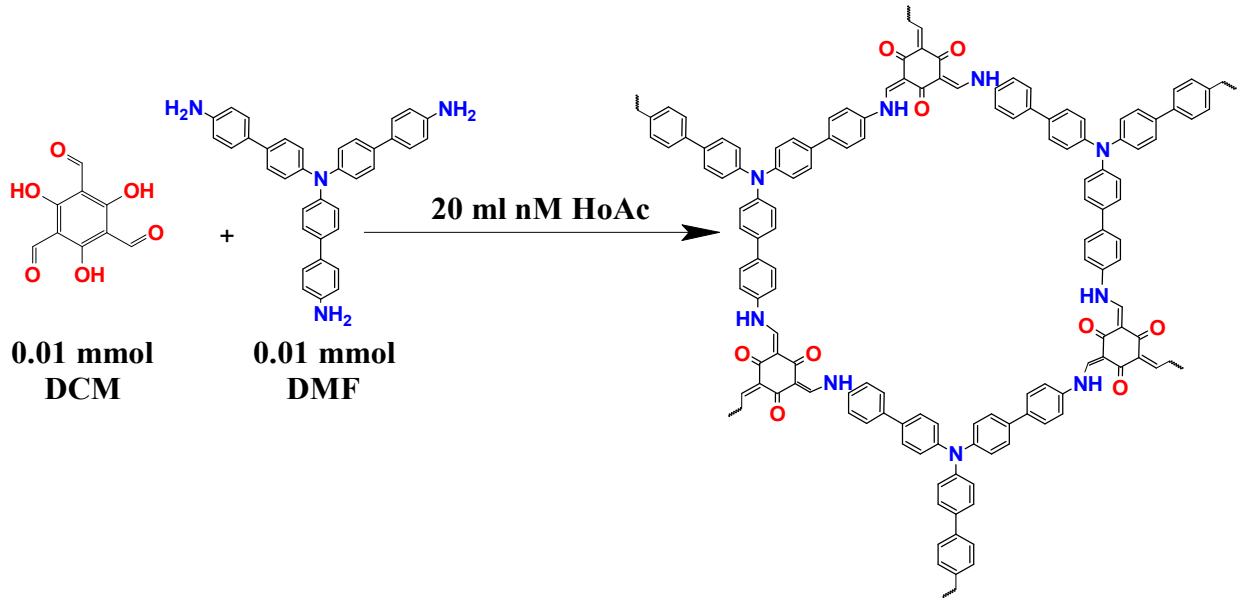

Scheme 1. Synthesis scheme of nM/Tp-NBD COFs synthesized via Liquid-Liquid interfacial method using 3, 6, 9, 12, 15 and 17 M acetic acid (HoAc).

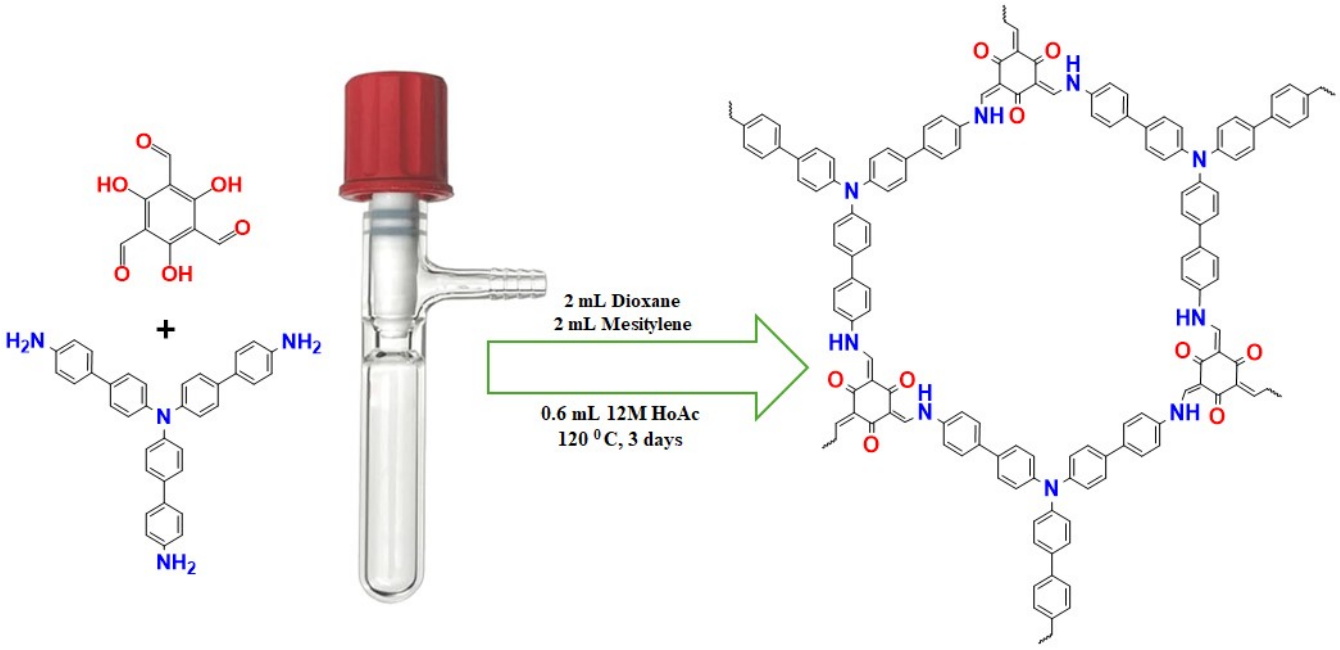

Scheme 2. Synthesis scheme for solvothermal synthesis of 12M/Tp-NBD COF using 12 M HoAc.

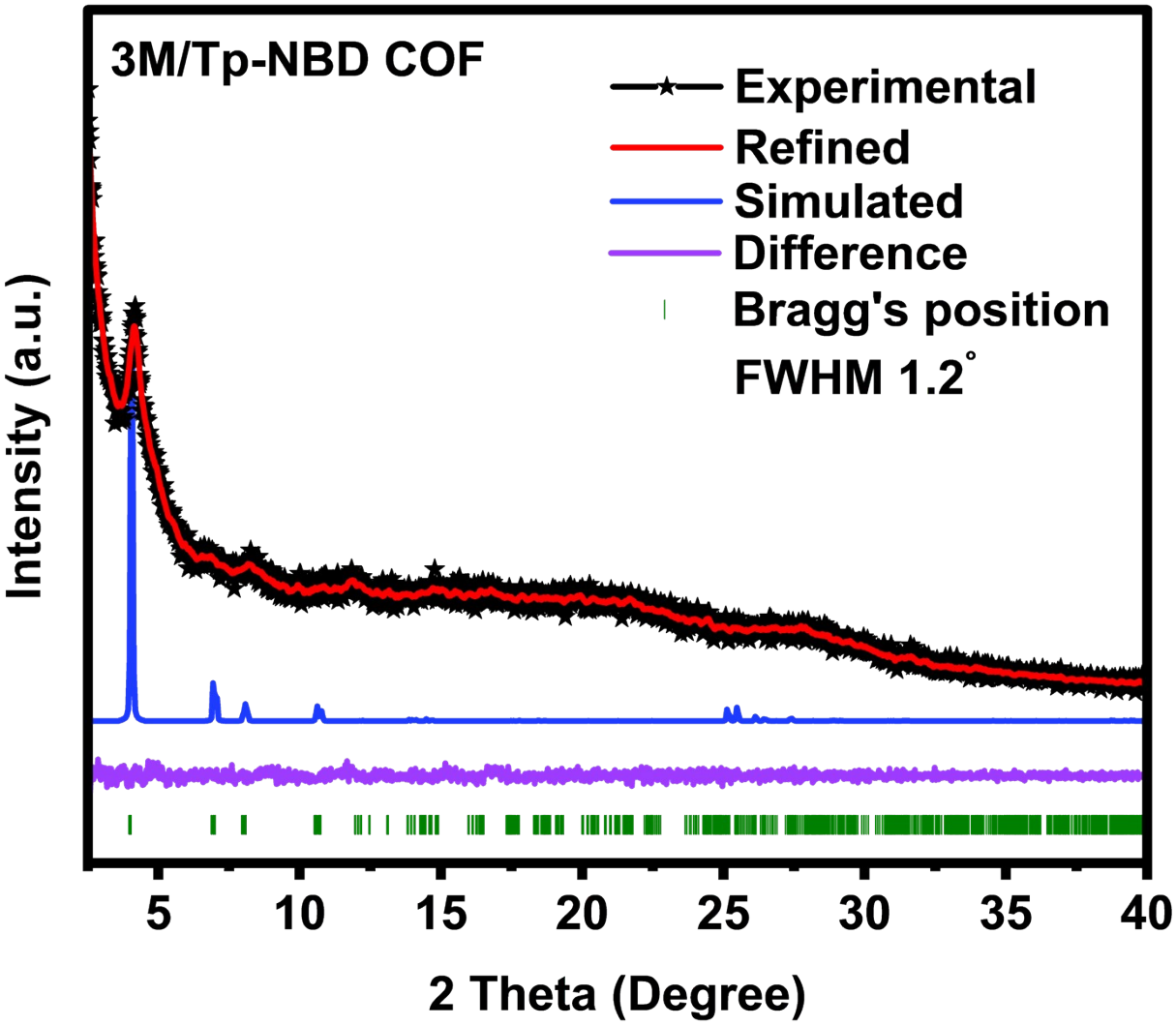

Figure S1. Experimental and Simulated PXRD patterns of 3M/Tp-NBD COF.

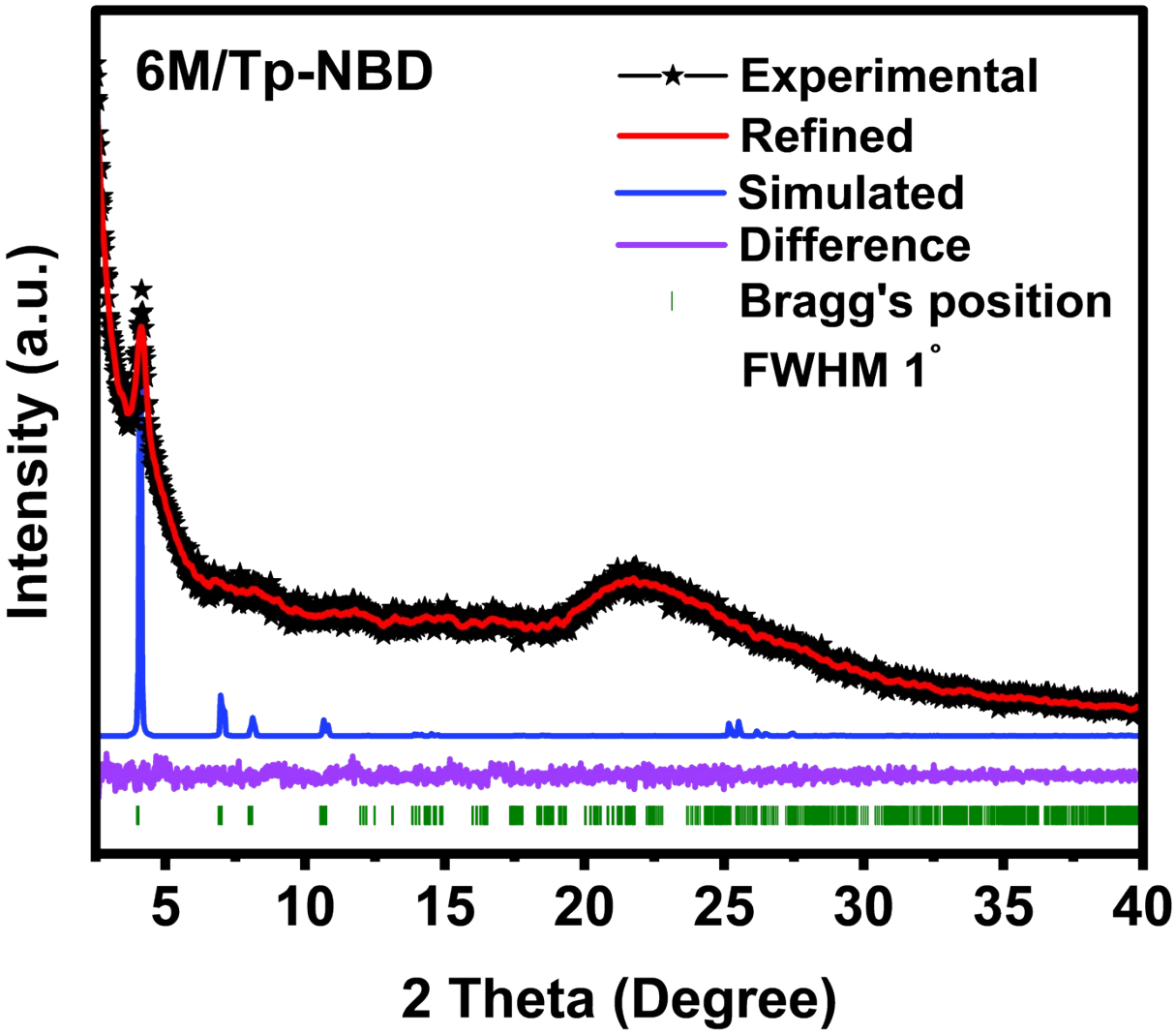

Figure S2. Experimental and Simulated PXRD patterns of 6M/Tp-NBD COF.

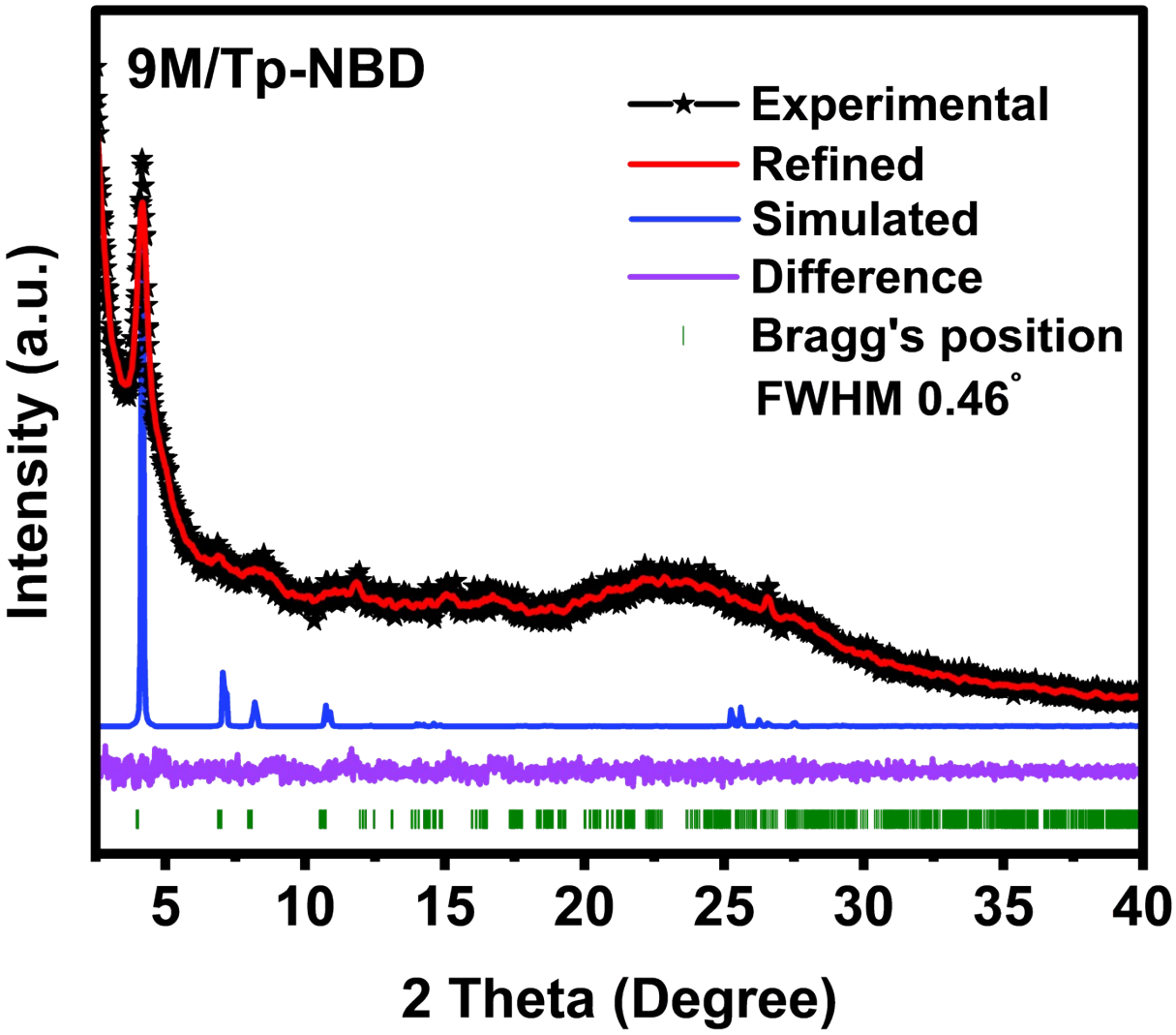

Figure S3. Experimental and Simulated PXRD patterns of 9M/Tp-NBD COF.

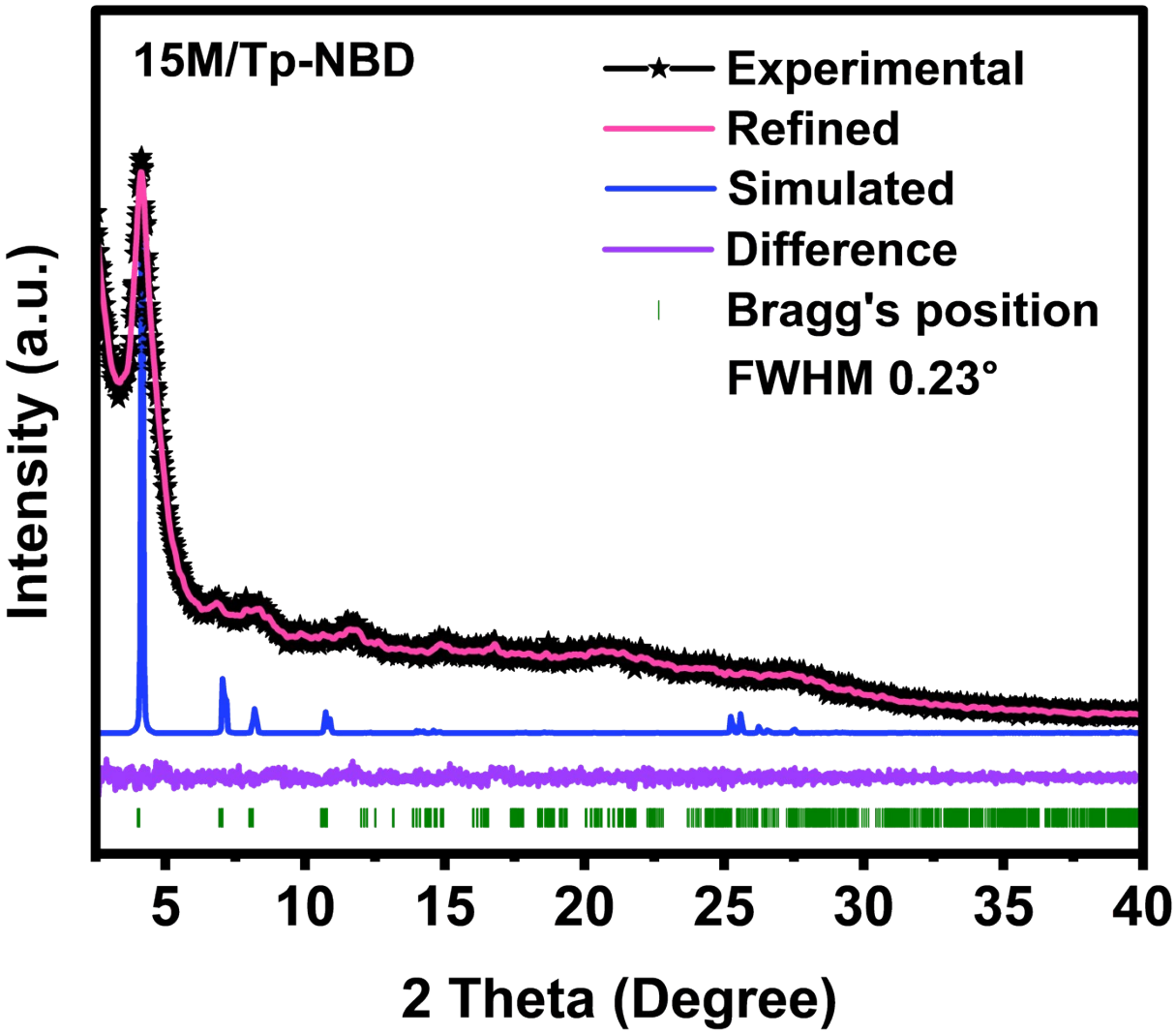

Figure S4. Experimental and Simulated PXRD patterns of 15M/Tp-NBD COF.

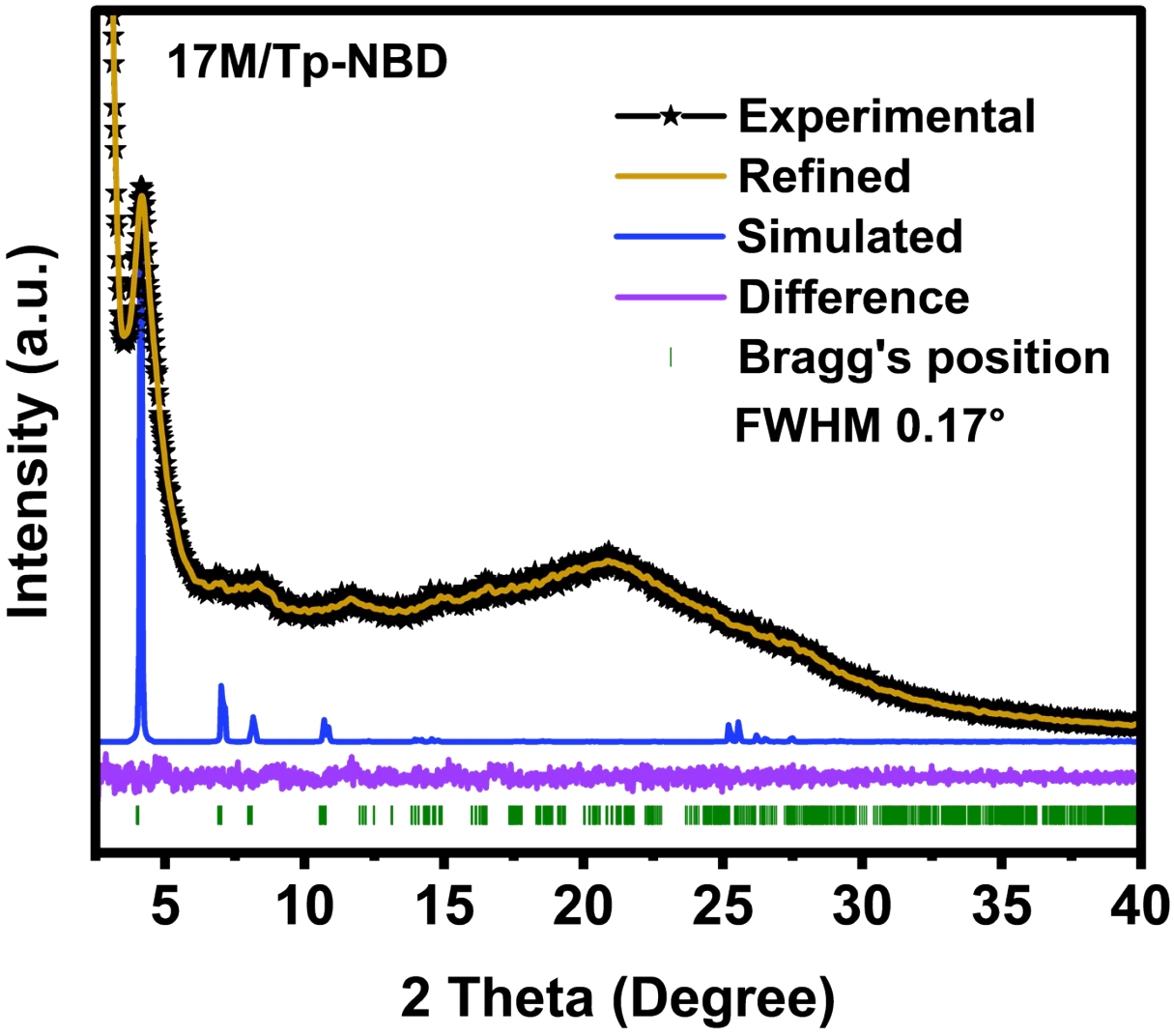

Figure S5. Experimental and Simulated PXRD patterns of 17M/Tp-NBD COF.

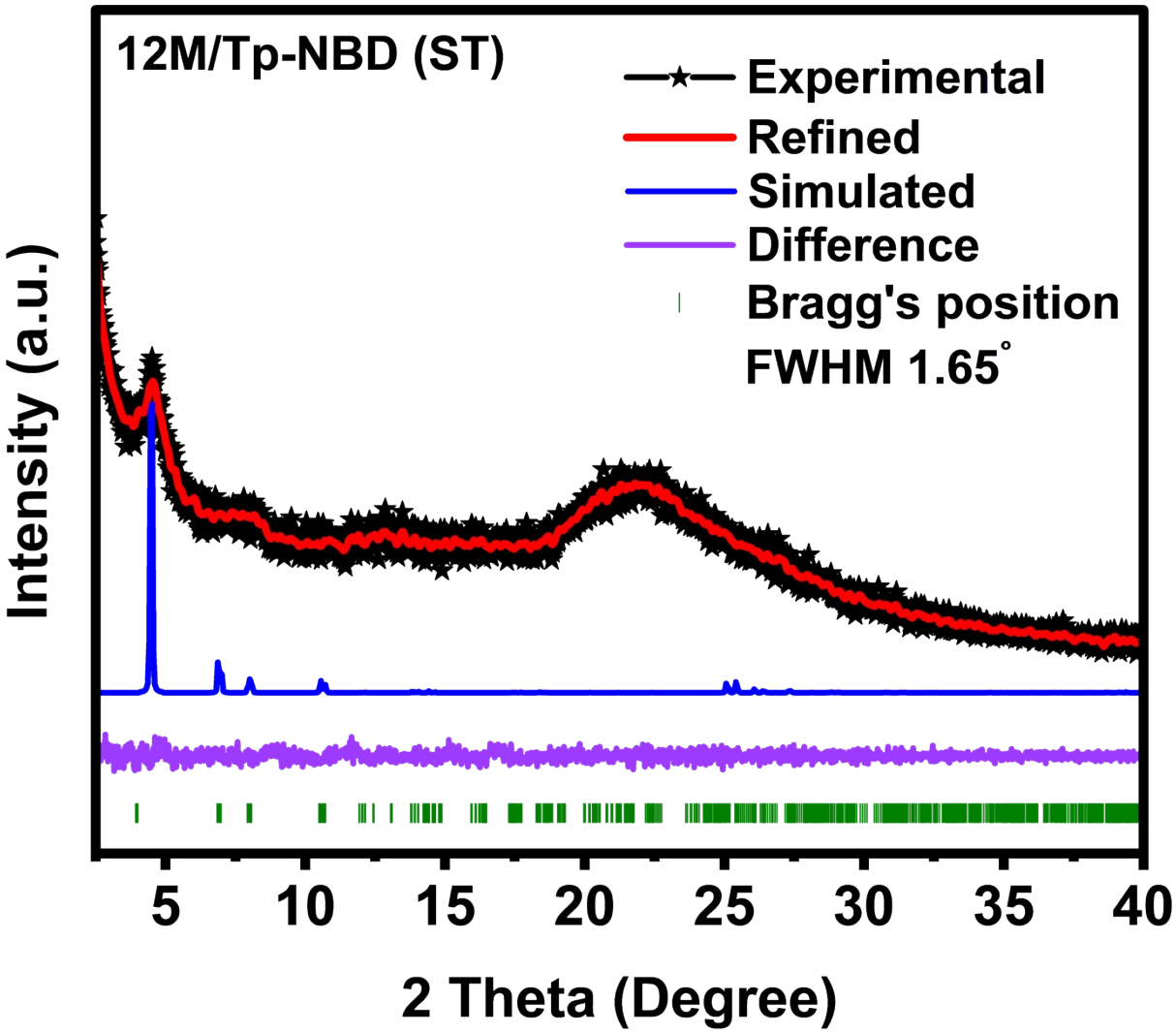

Figure S6. Experimental and Simulated PXRD patterns of 12M/Tp-NBD (ST) COF synthesized via the Solvothermal (ST) method.

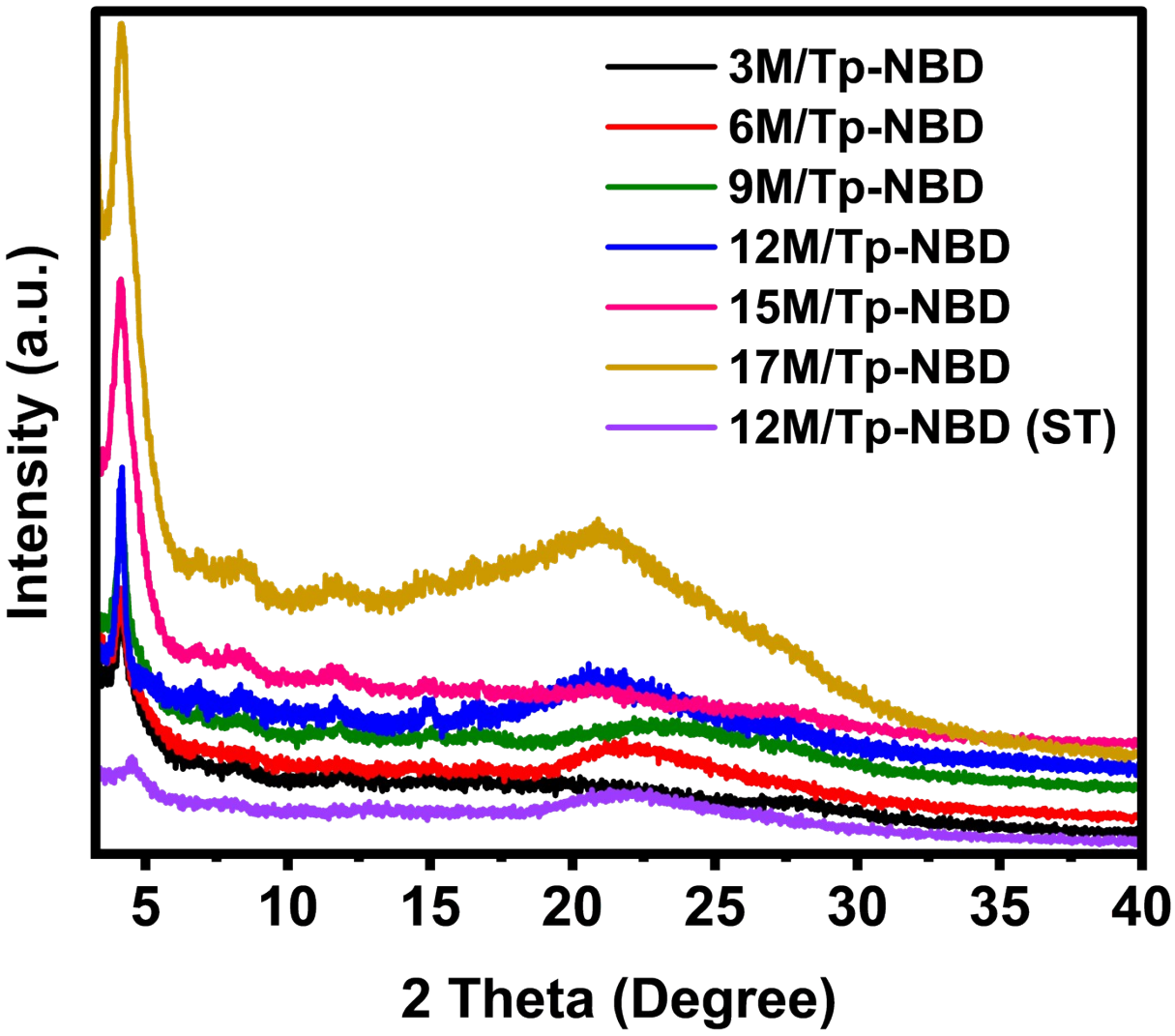

Figure S7. Comparison of Experimental PXRD peak patterns of 3-17M/Tp-NBD COFs synthesized via the Liquid-Liquid Interfacial (LLI) method, 12M/Tp-NBD (ST) COF synthesized via the Solvothermal (ST) method.

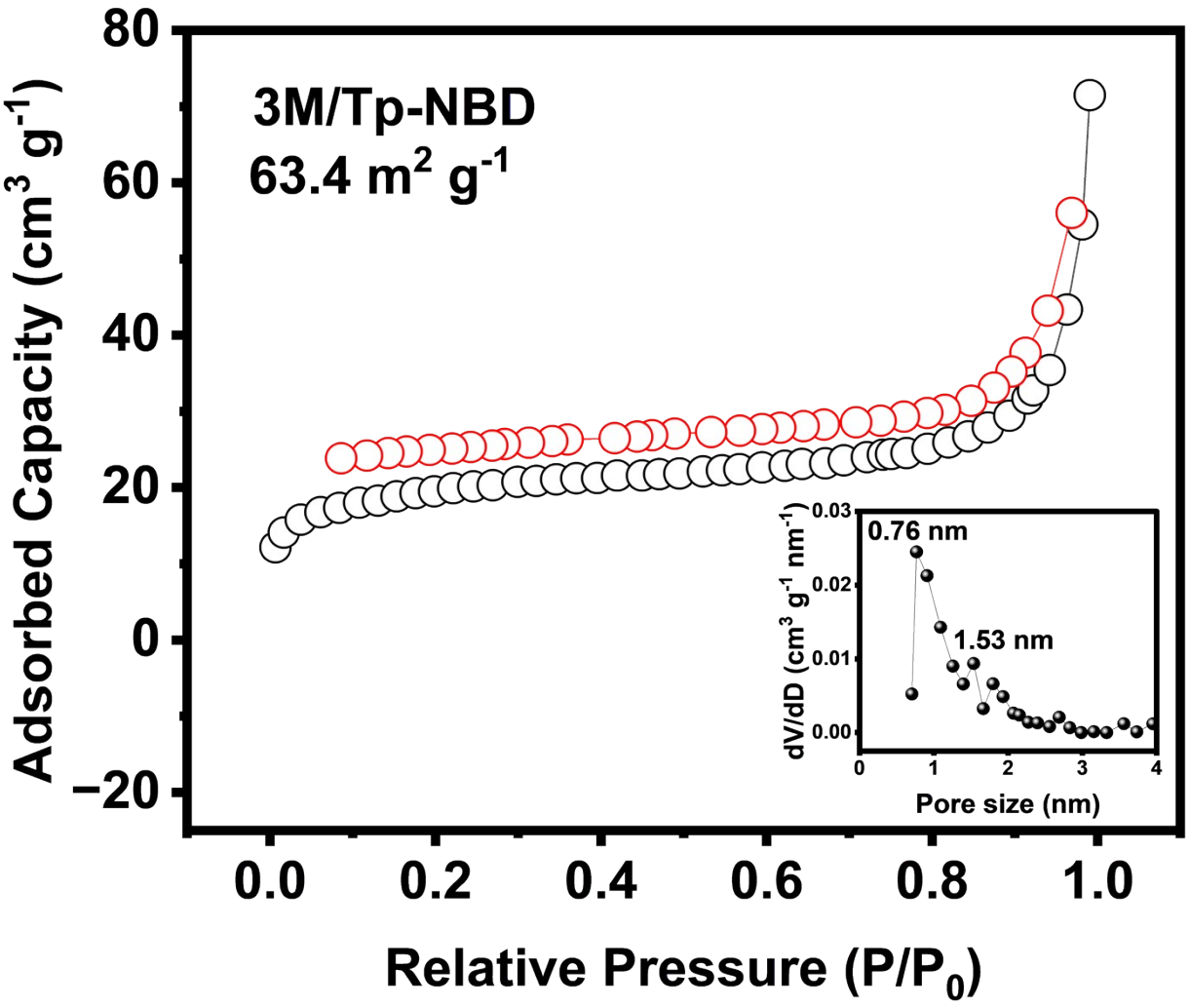

Figure S8. N_2 adsorption-desorption isotherm (Inset: pore size distribution by NLDFT method) of 3M/Tp-NBD COF.

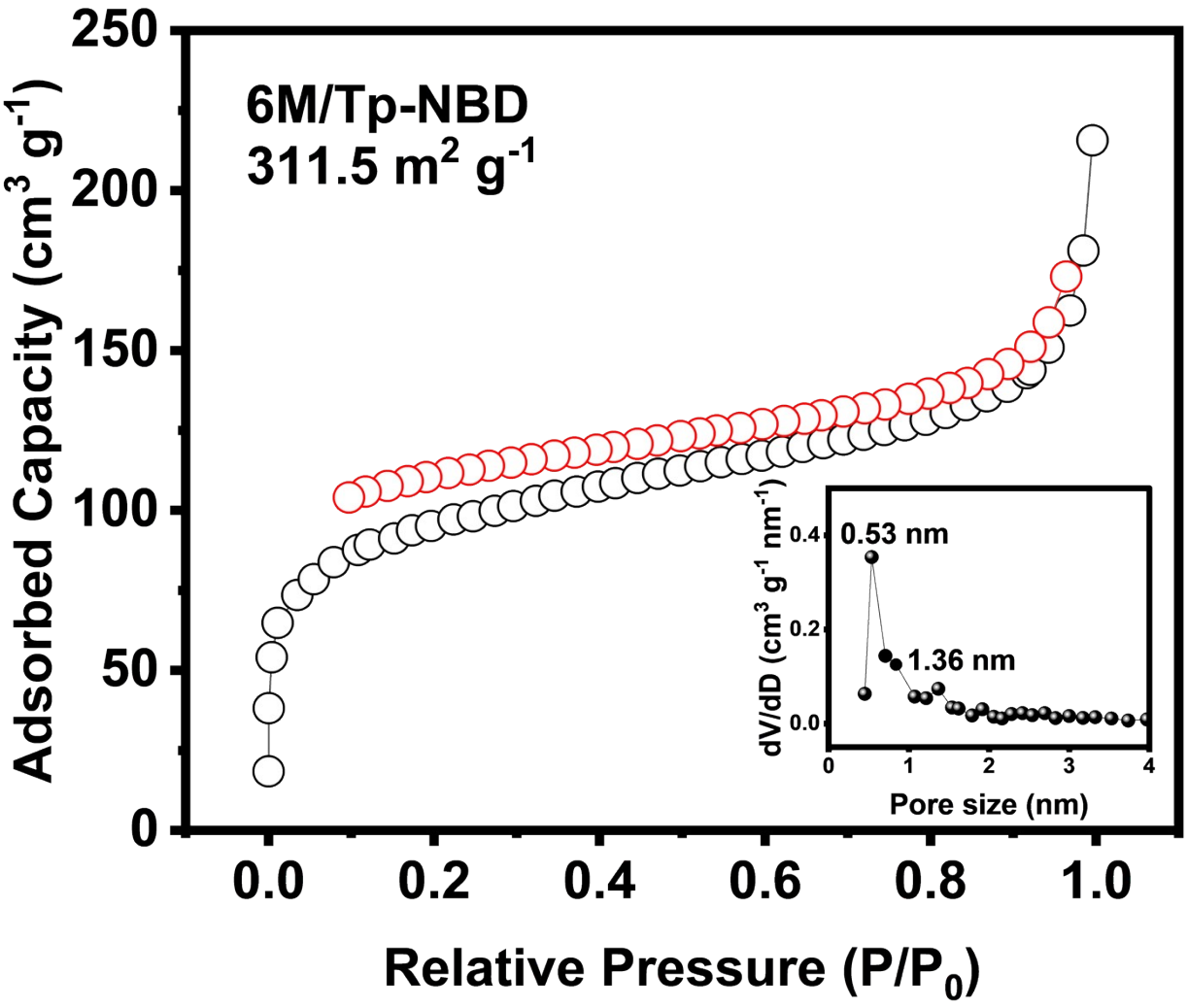

Figure S9. N_2 adsorption-desorption isotherm (Inset: pore size distribution by NLDFT method) of 6M/Tp-NBD COF.

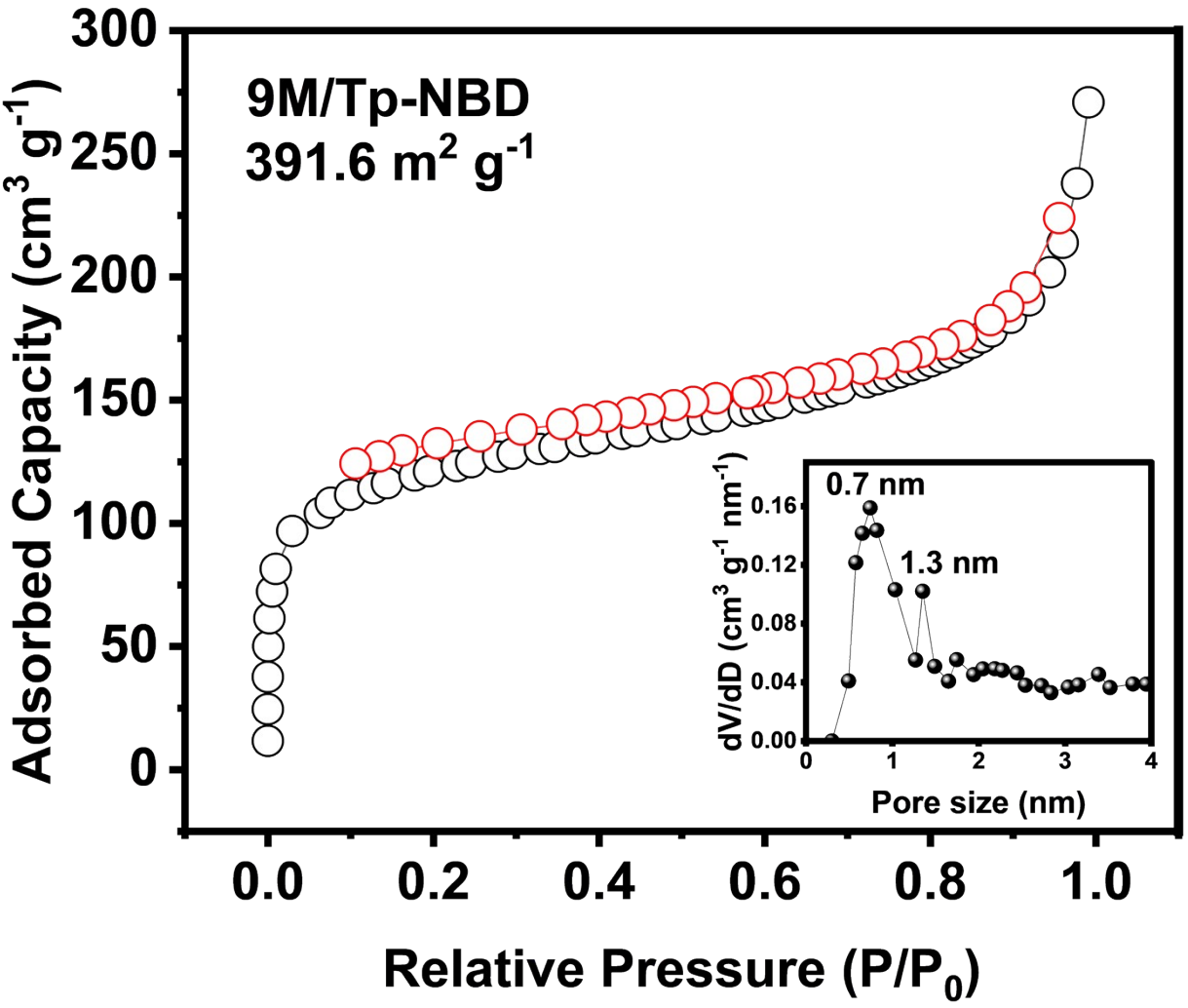

Figure S10. N_2 adsorption-desorption isotherm (Inset: pore size distribution by NLDFT method) of 9M/Tp-NBD COF.

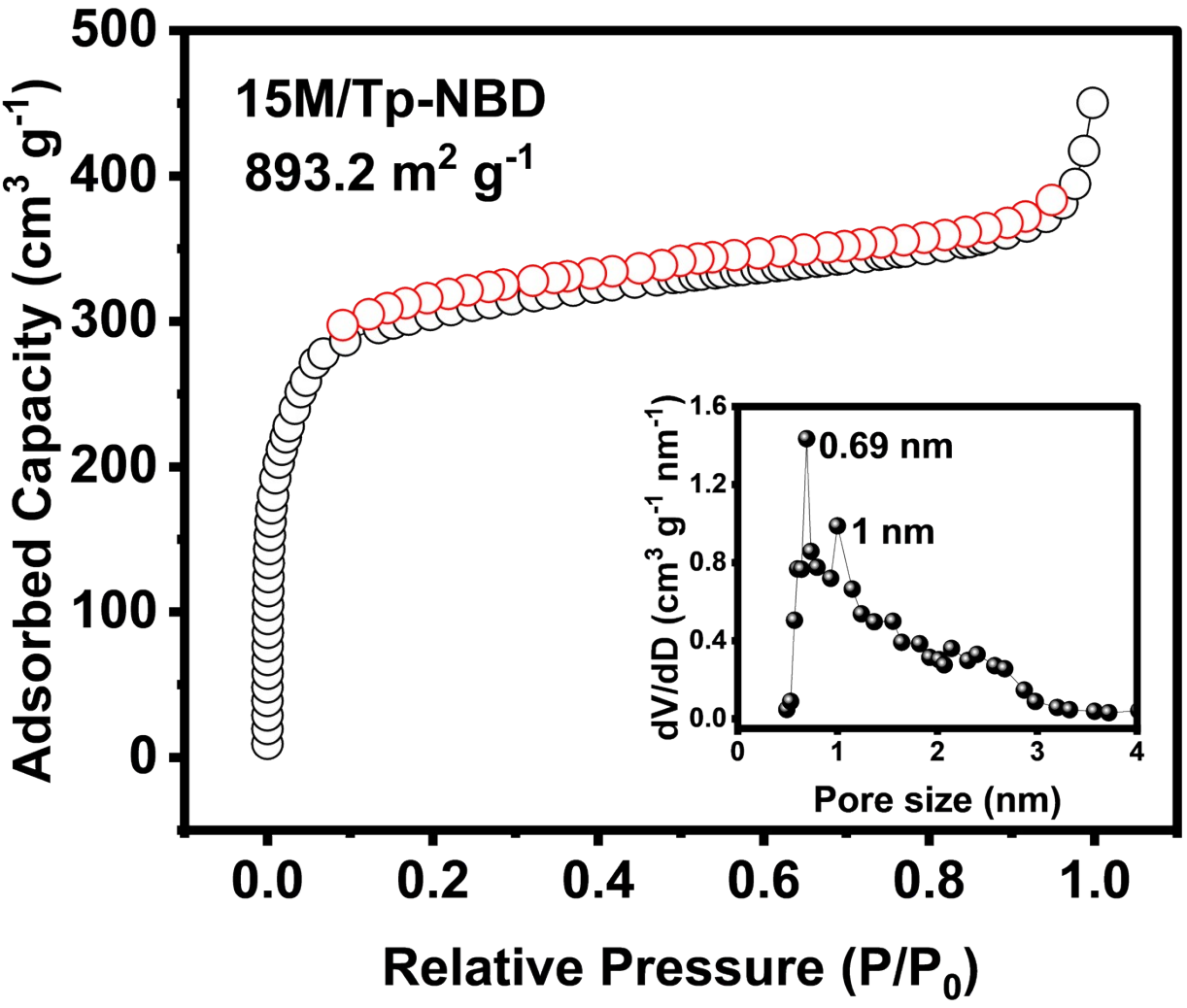

Figure S11. N_2 adsorption-desorption isotherm (Inset: pore size distribution by NLDFT method) of 15M/Tp-NBD COF.

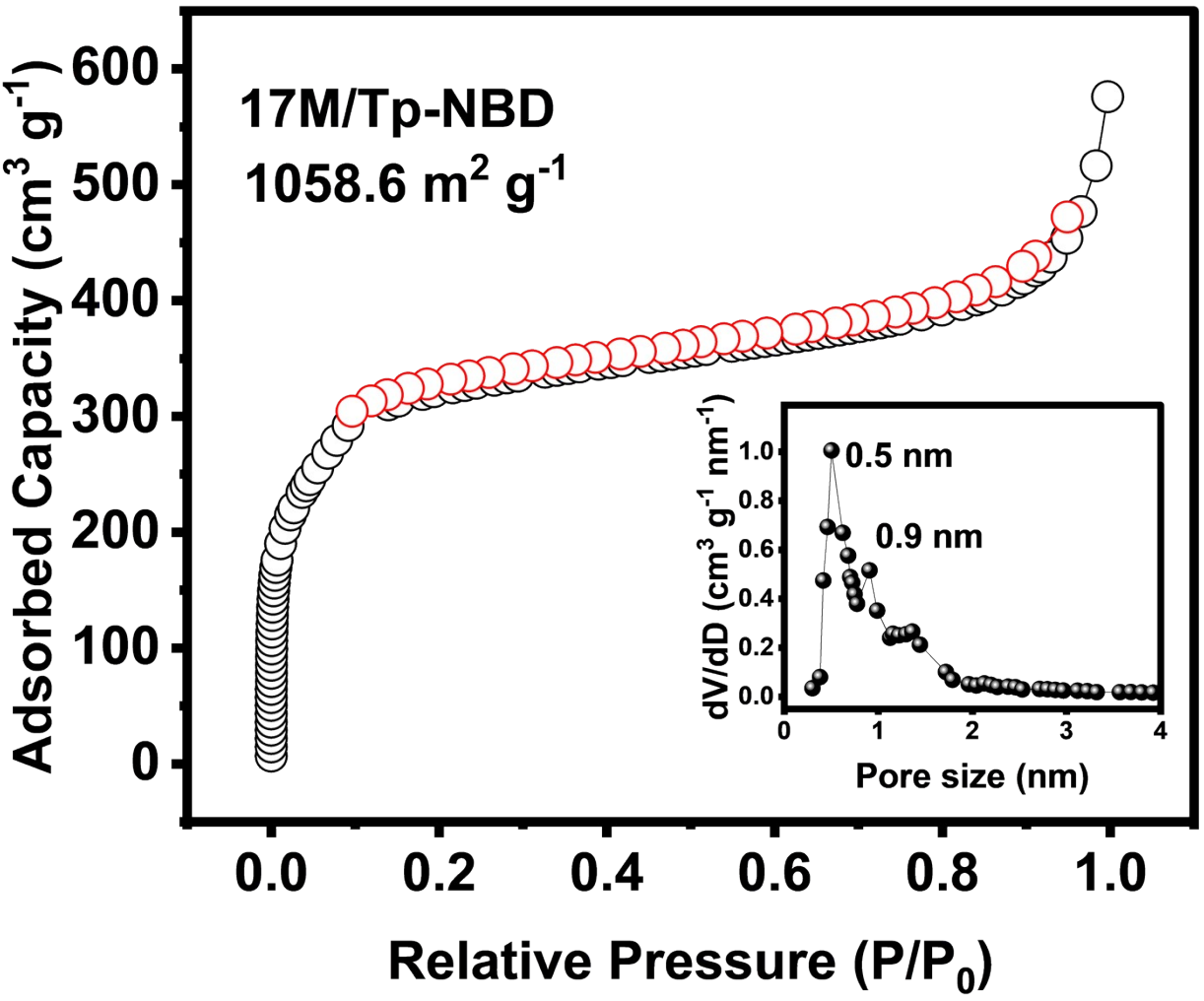

Figure S12. N_2 adsorption-desorption isotherm (Inset: pore size distribution by NLDFT method) of 17M/Tp-NBD COF.

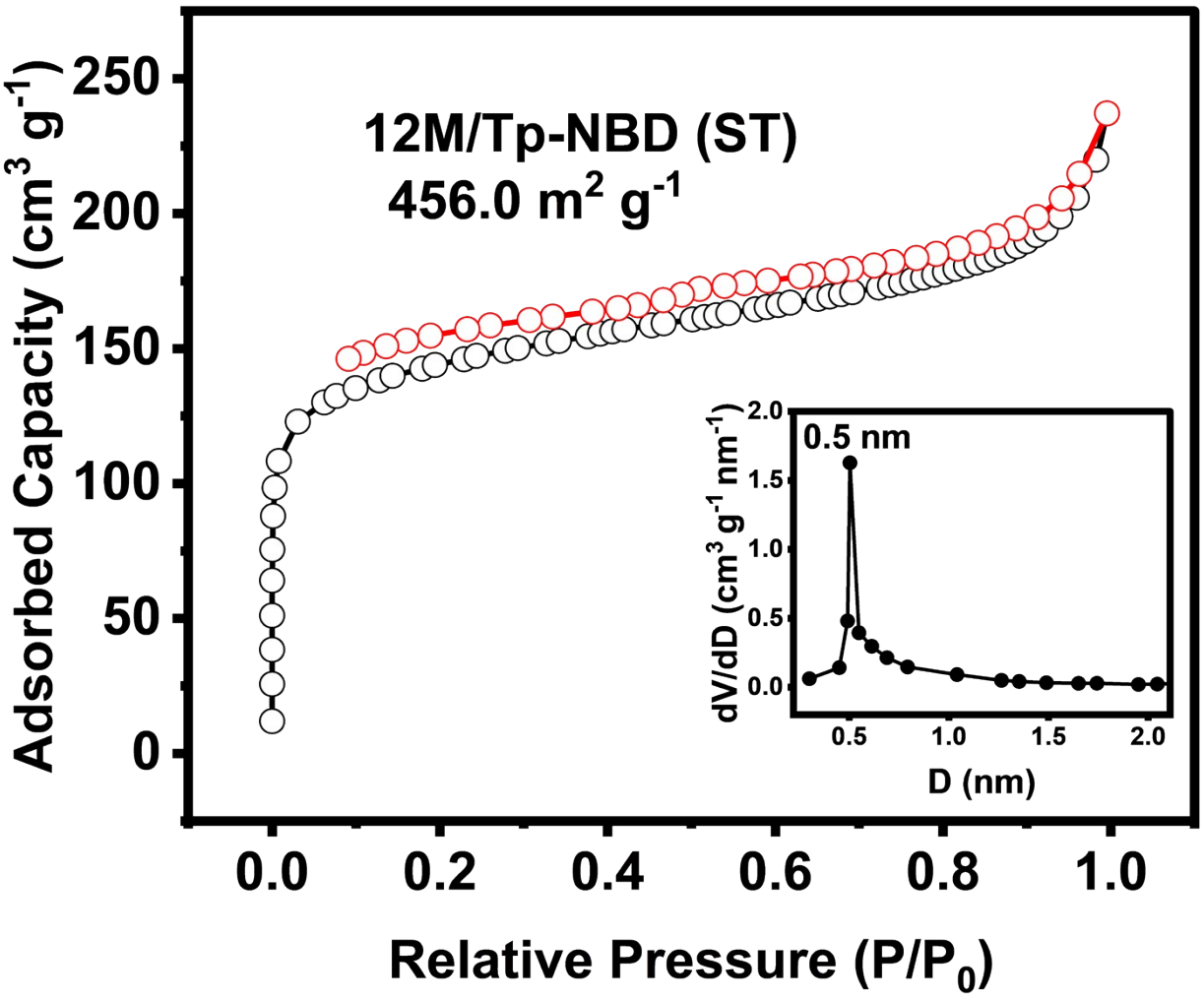

Figure S13. N_2 adsorption-desorption isotherm (Inset: pore size distribution by NLDFT method) of 12M/Tp-NBD (ST) COF.

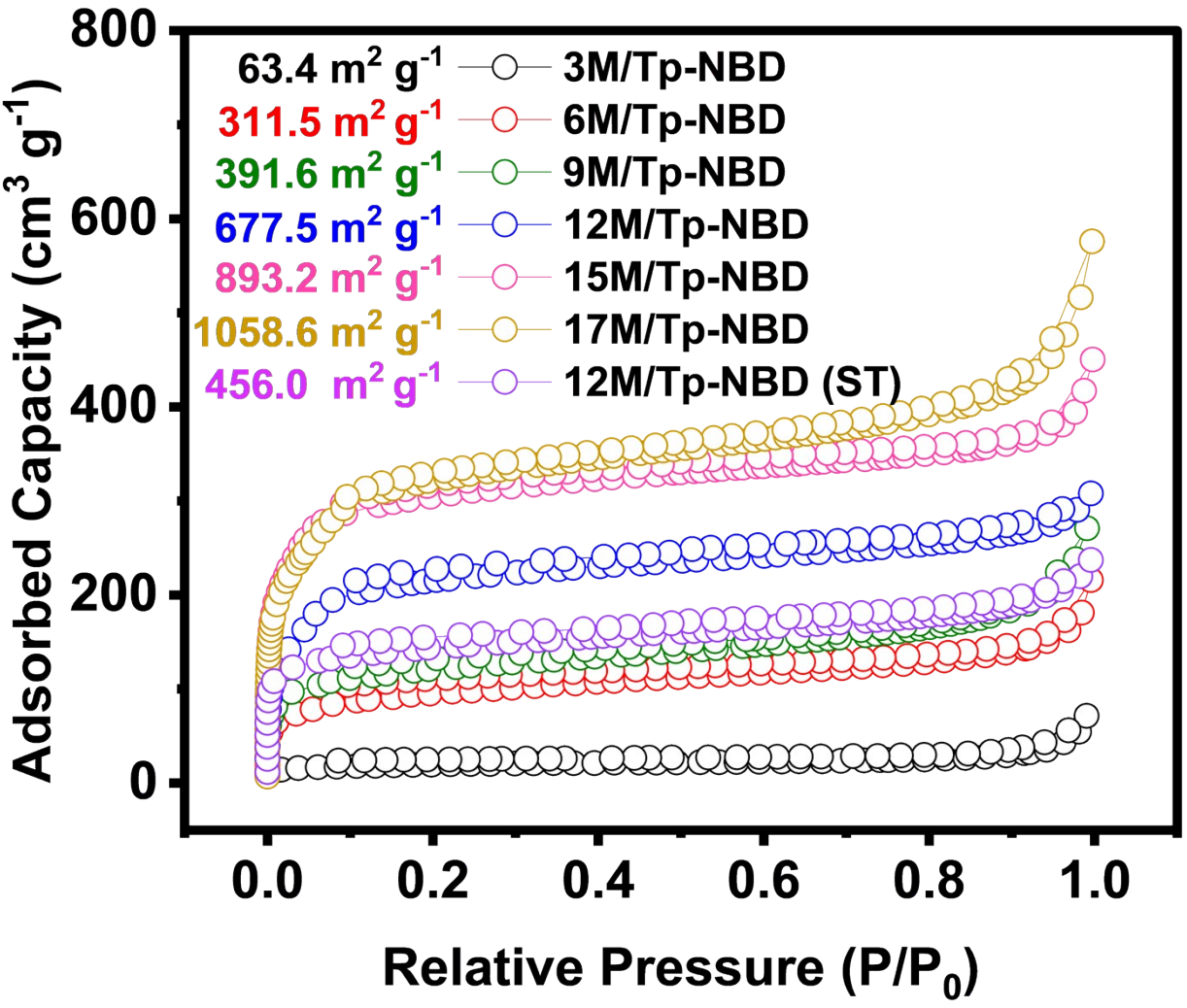

Figure S14. Comparative N_2 adsorption-desorption isotherms of 3-17M/Tp-NBD and 12M/Tp-NBD (ST) COFs (The corresponding BET surface area and pore size distribution data are summarized in Table S1).

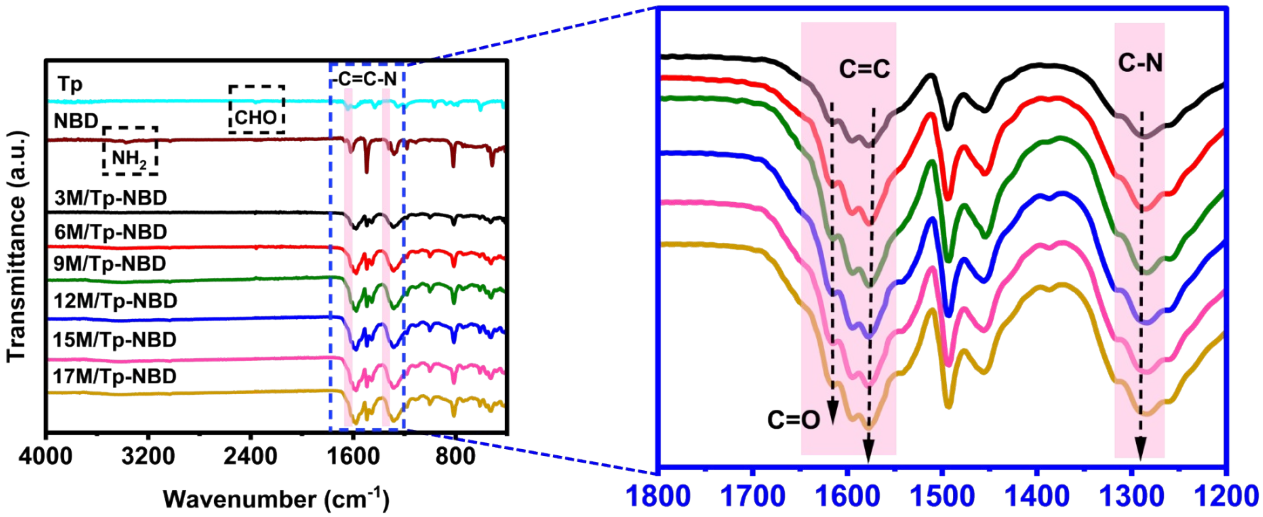

Figure S15. Comparative FT-IR spectra of 3-17M/Tp-NBD (LLI) COFs.

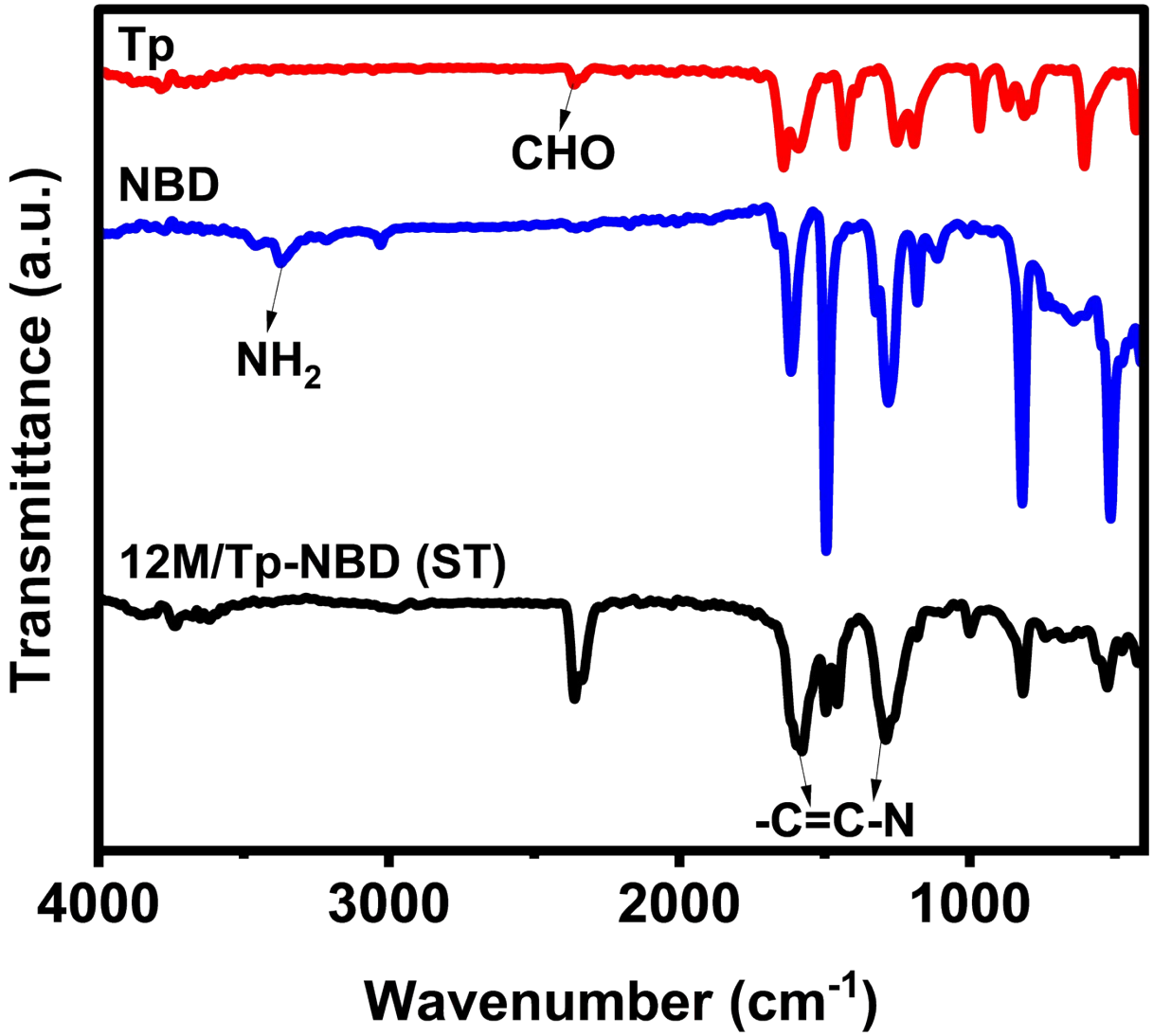

Figure S16. FT-IR spectra of 12M/Tp-NBD (ST) COF.

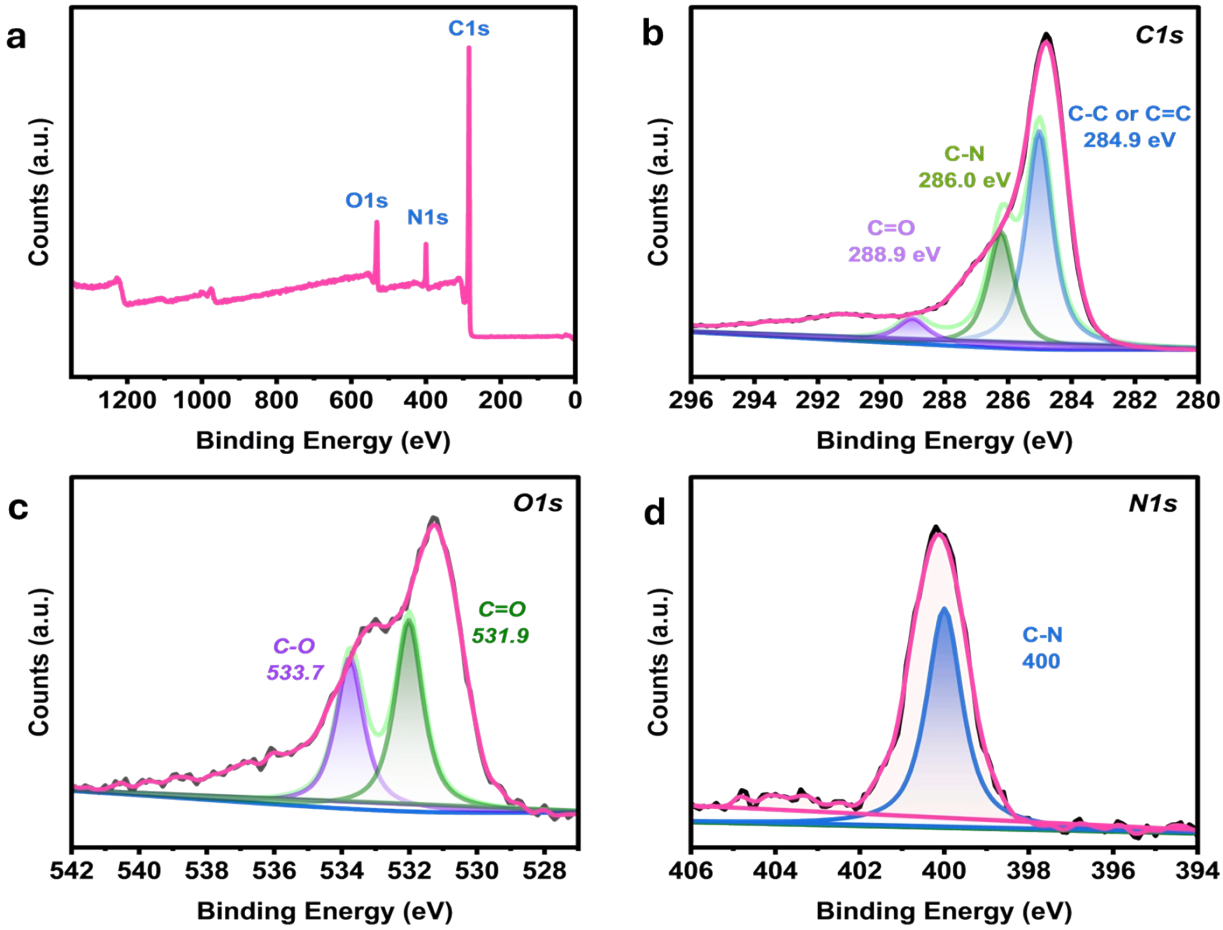

Figure S17. (a) XPS survey; and High-resolution XPS spectra of (b) C1s, (c) N1s, (d) O1s scans of 12M/Tp-NBD COF.

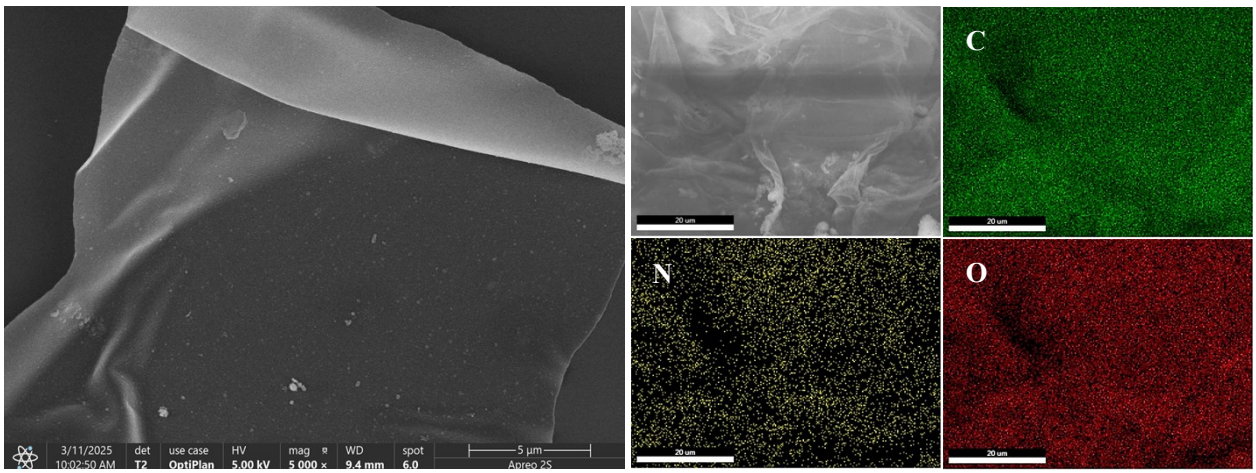

Figure S18. SEM image and elemental mapping images for C, N, and O of 3M/Tp-NBD COF.

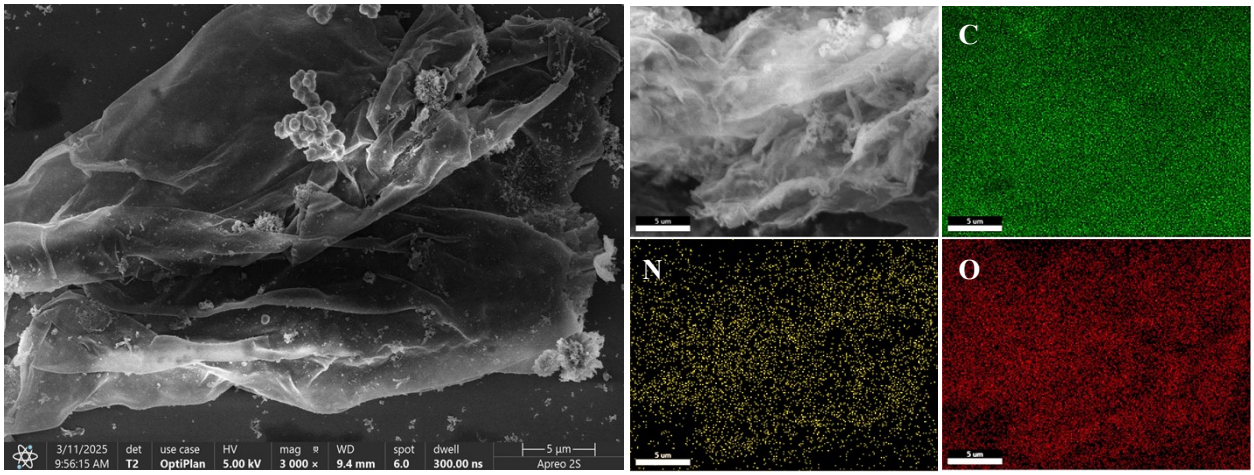

Figure S19. SEM image and elemental mapping images for C, N, and O of 6M/Tp-NBD COF.

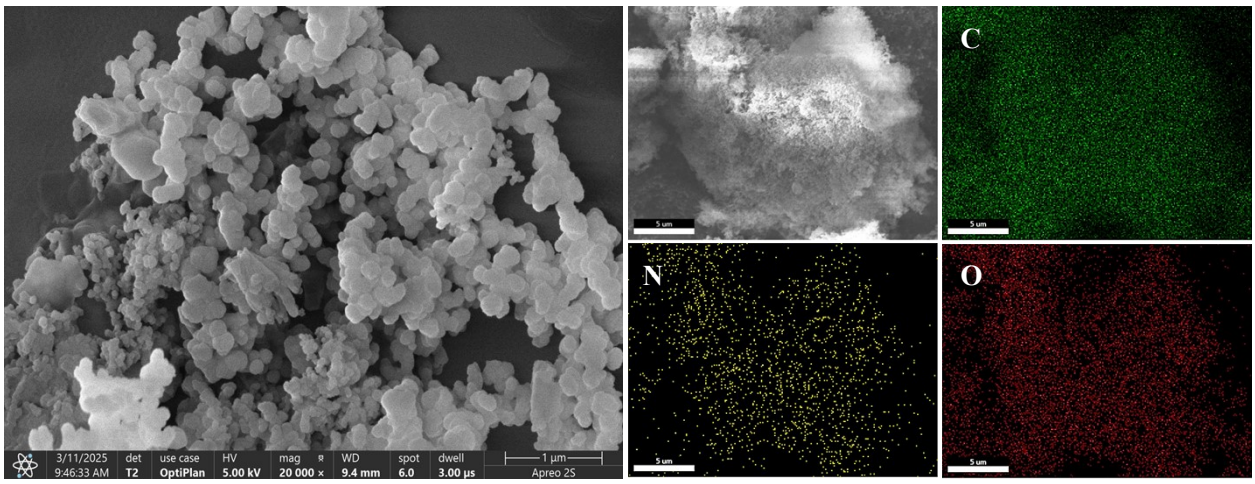

Figure S20. SEM image and elemental mapping images for C, N, and O of 9M/Tp-NBD COF.

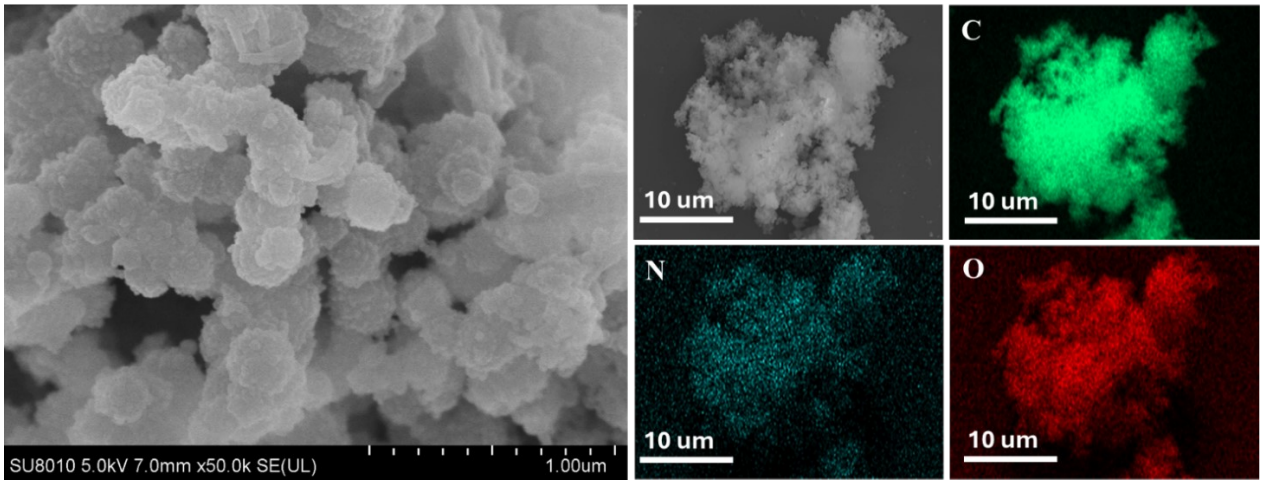

Figure S21. SEM image and elemental mapping images for C, N, and O of 15M/Tp-NBD COF.

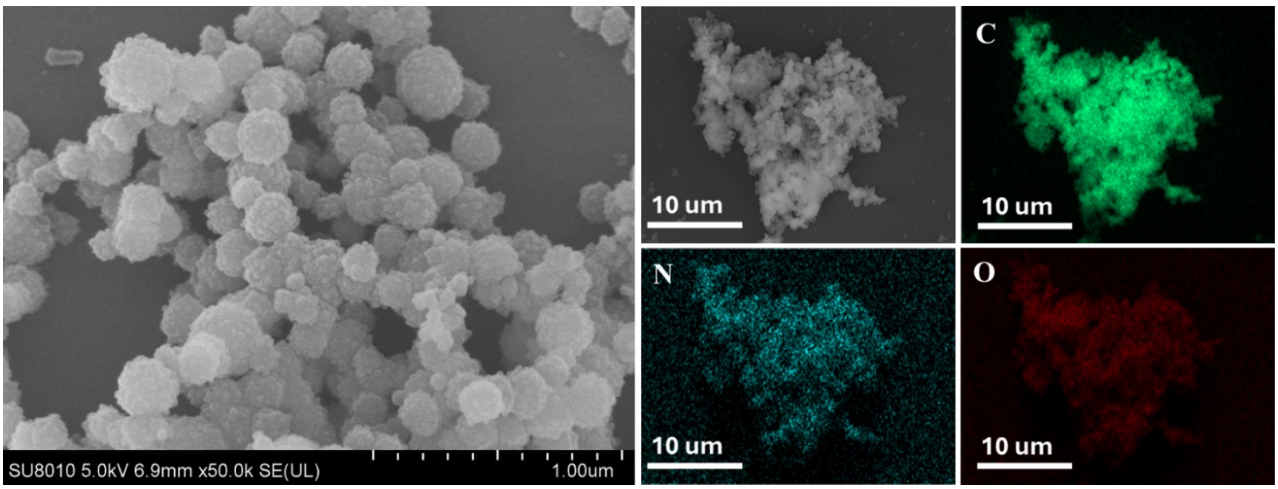

Figure S22. SEM image and elemental mapping images for C, N, and O of 17M/Tp-NBD COF.

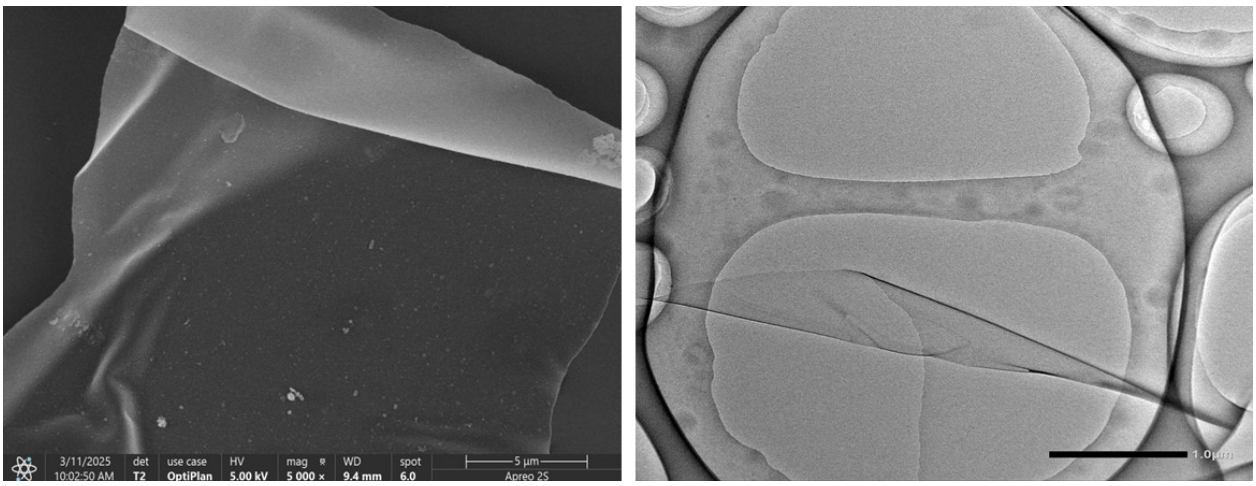

Figure S23. SEM and TEM images of 3M/Tp-NBD COF.

Figure S24. SEM and TEM images of 6M/Tp-NBD COF.

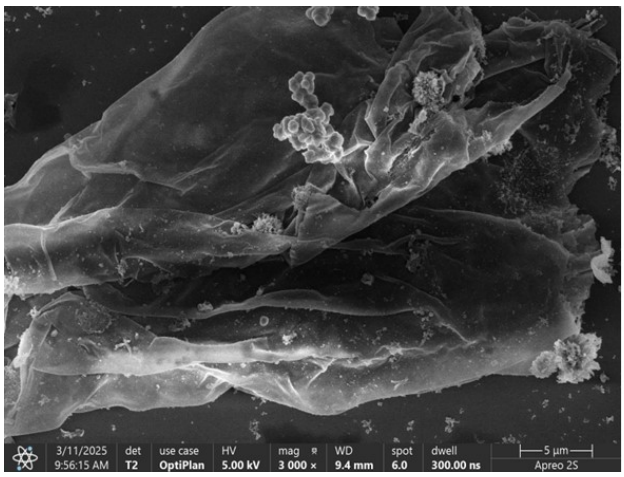
3/11/2025
9:56:15 AM
det
T2
use case
OptiPlan
HV
5.00 kV
mag
3 000 x
WD
9.4 mm
spot
6.0
dwell
300.00 ns
5 µm
Apreo 2S

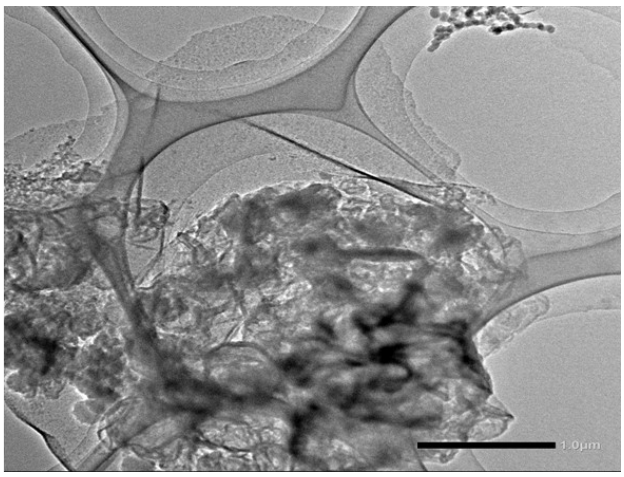
1.0µm

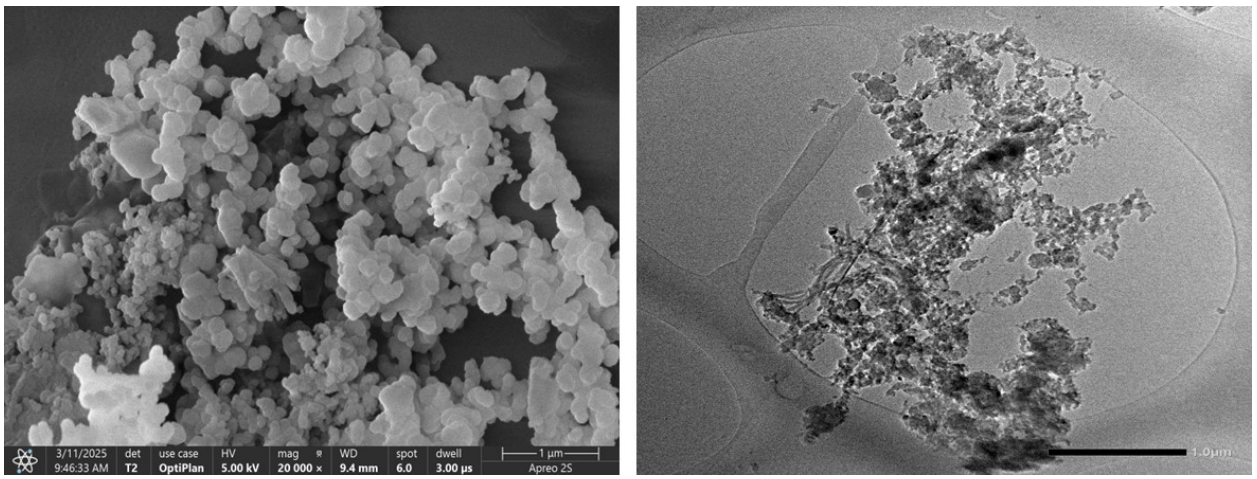

Figure S25. SEM and TEM images of 9M/Tp-NBD COF.

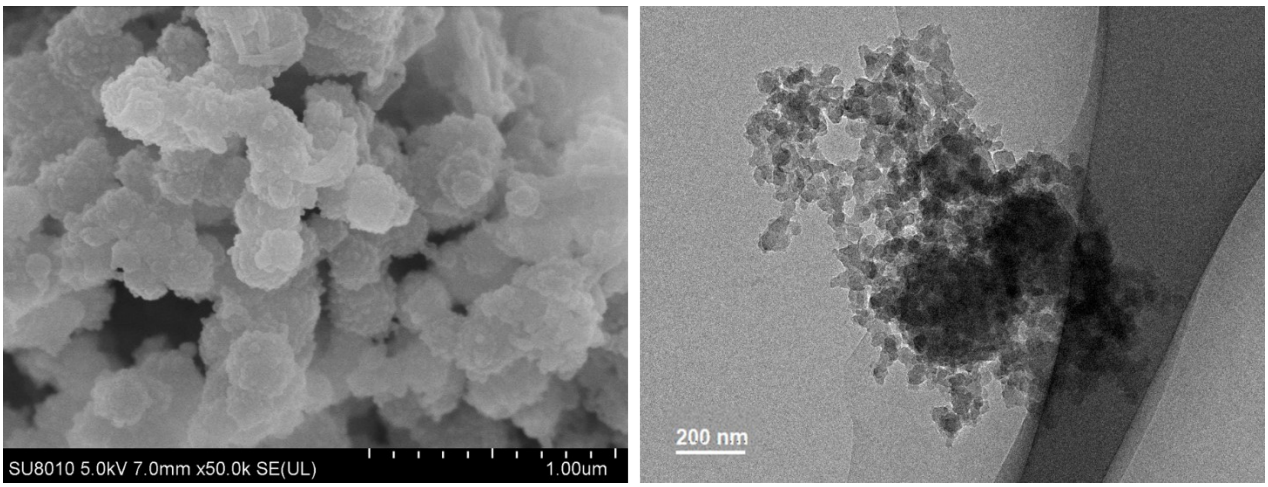

Figure S26. SEM and TEM images of 15M/Tp-NBD COF.

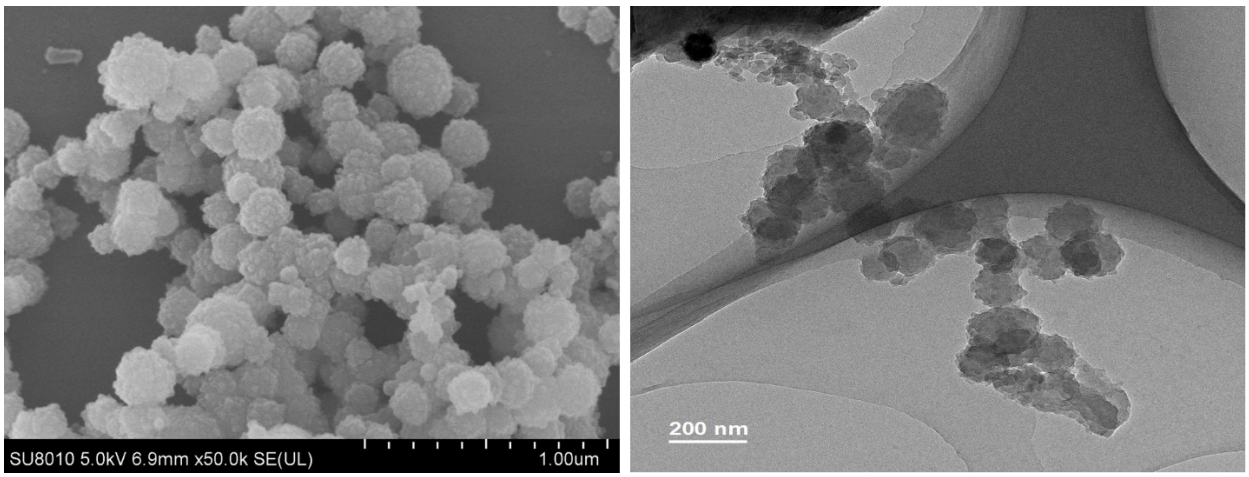

Figure S27. SEM and TEM images of 17M/Tp-NBD COF.

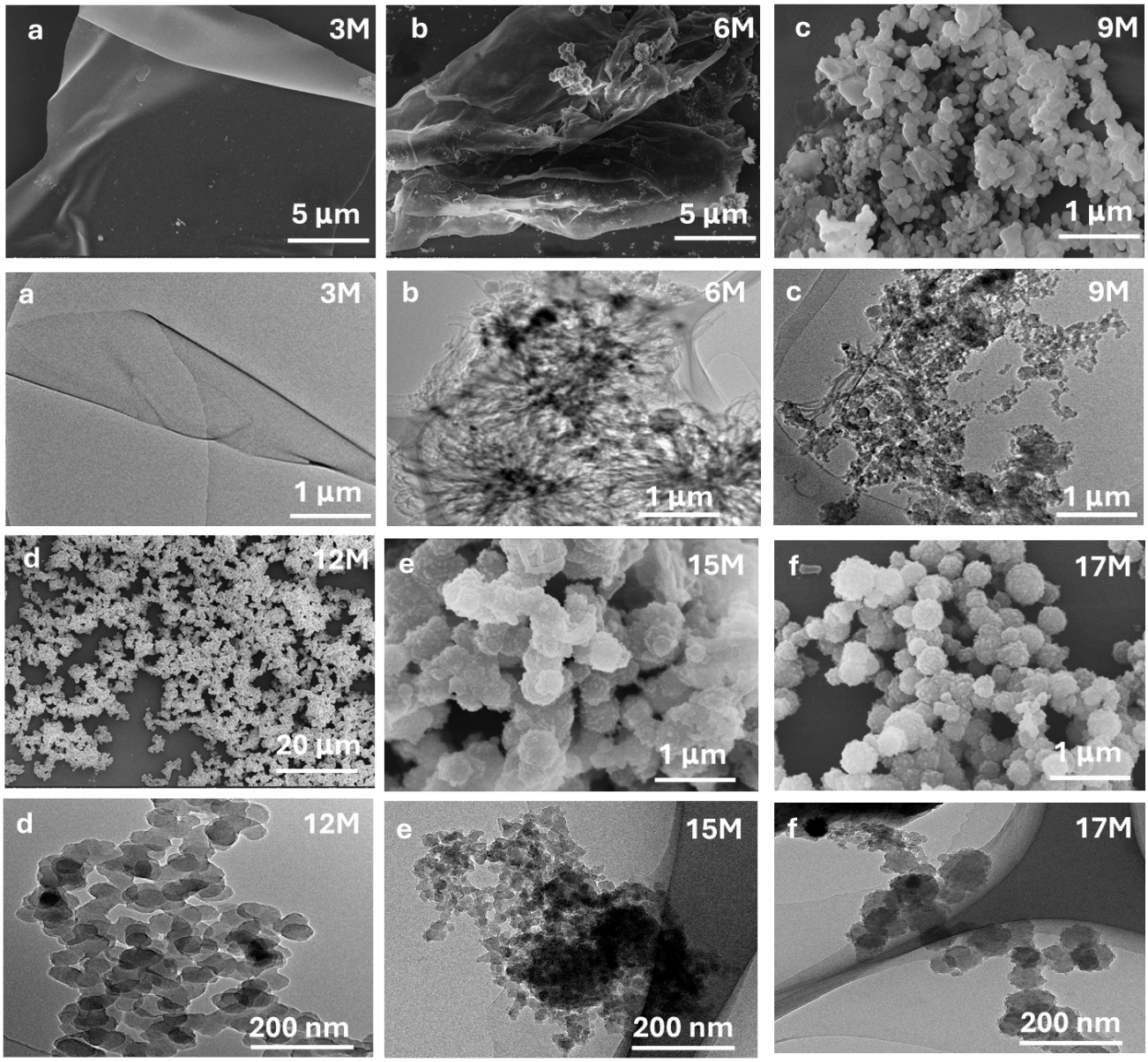

Figure S28. SEM and TEM images of (a) 3M/Tp-NBD; (b) 6M/Tp-NBD; (c) 9M/Tp-NBD; (d) 12M/Tp-NBD; (e) 15M/Tp-NBD; and (f) 17M/Tp-NBD COFs for comparison of morphologies.

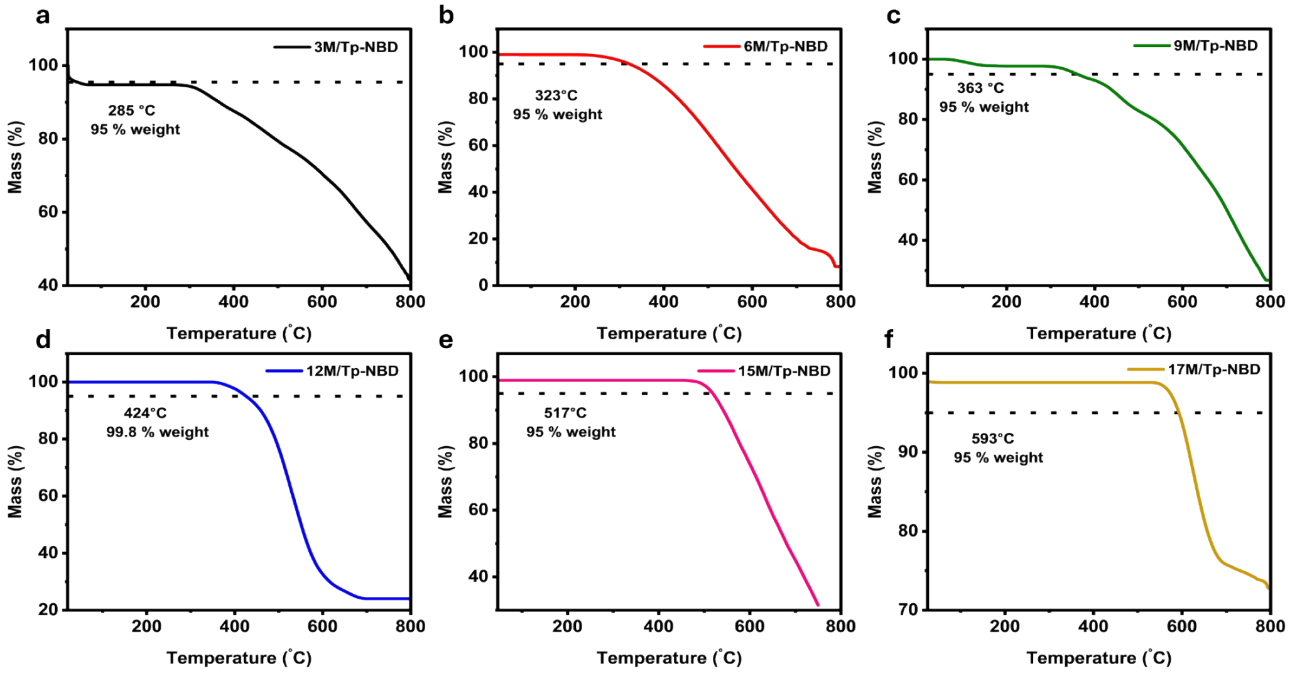

Figure S29. TGA profiles of (a) 3M/Tp-NBD COF; (b) 6M/Tp-NBD COF; (c) 9M/Tp-NBD COF; (d) 12M/Tp-NBD COF; (e) 15M/Tp-NBD COF; and (f) 17M/Tp-NBD COF.

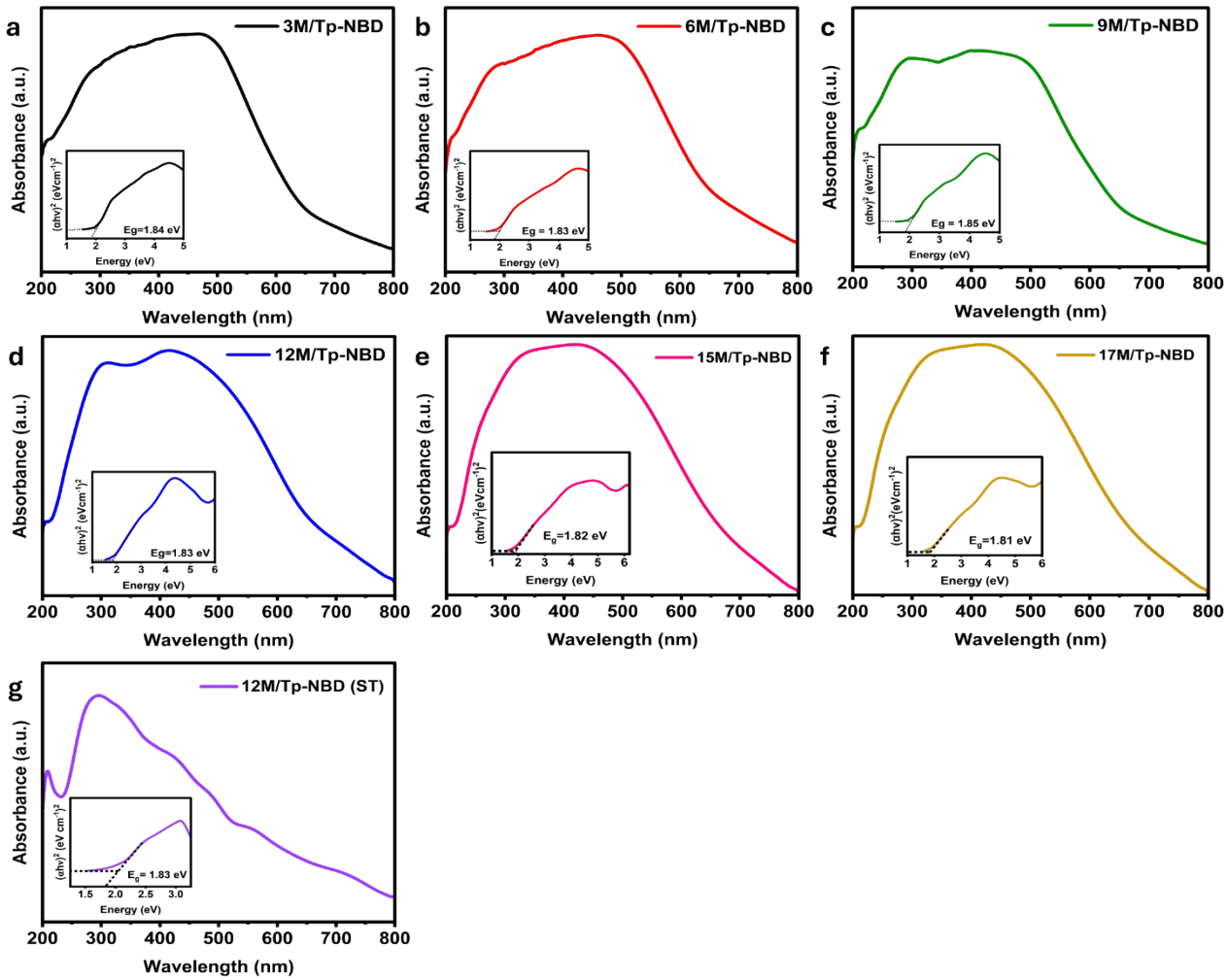

Figure S30. UV-vis DRS spectra (Insets: Tauc plots) of (a) 3M/Tp-NBD COF; (b) 6M/Tp-NBD COF; (c) 9M/Tp-NBD COF; (d) 12M/Tp-NBD COF; (e) 15M/Tp-NBD COF; (f) 17M/Tp-NBD COF; and (g) 12M/Tp-NBD (ST) COF.

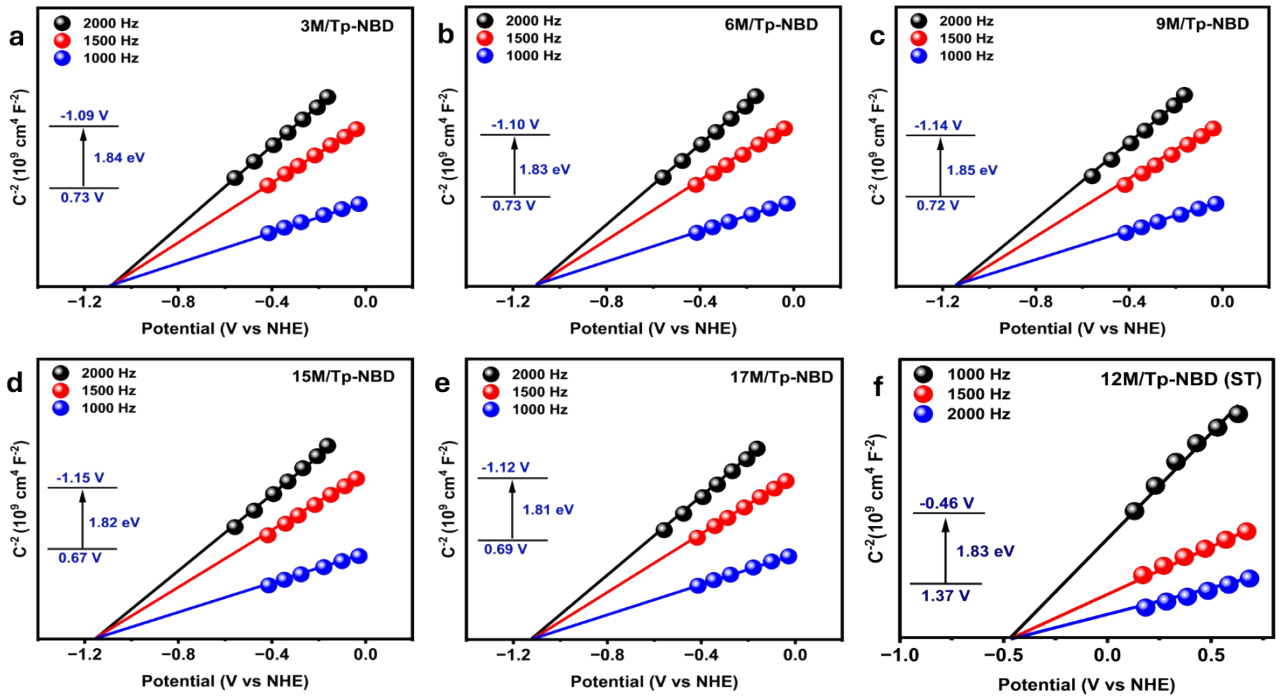

Figure S31. Mott-Schottky plot (Inset: flat band potential (E_{fb})) of (a) 3M/Tp-NBD COF; (b) 6M/Tp-NBD COF; (c) 9M/Tp-NBD COF; (d) 12M/Tp-NBD COF; (e) 15M/Tp-NBD COF; (f) 17M/Tp-NBD COF; and (g) 12M/Tp-NBD (ST) COF.

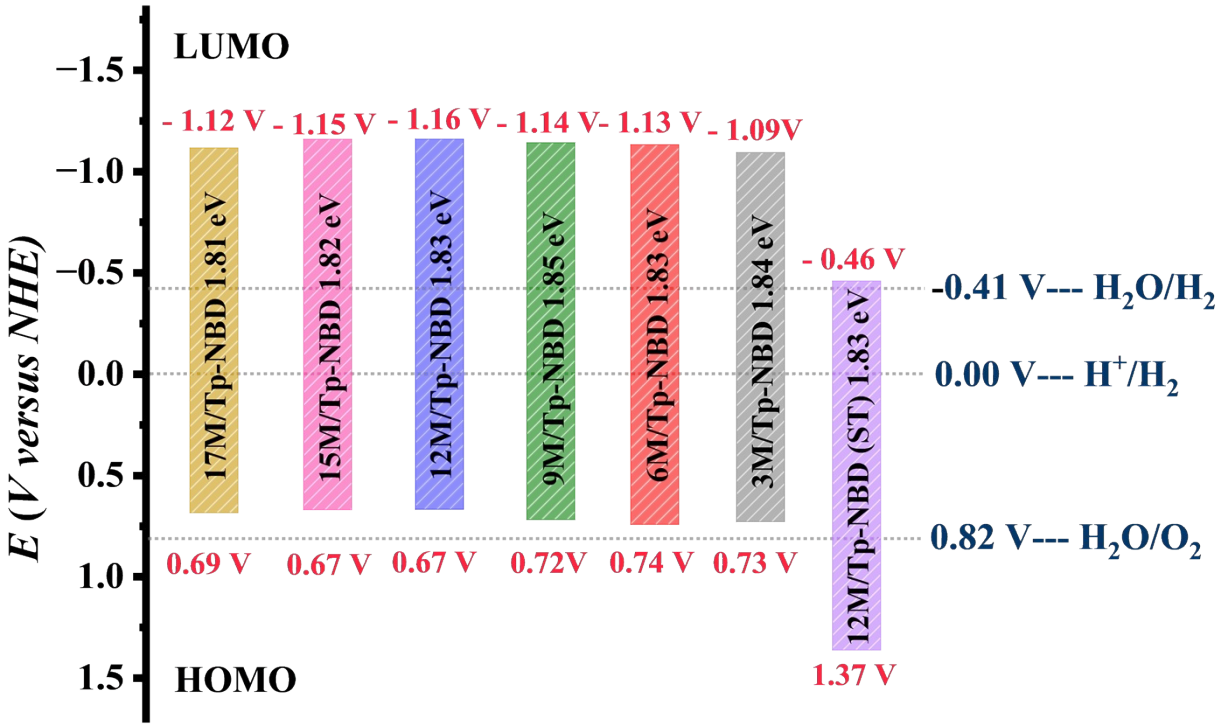

Figure S32. Energy band gap measurements of HOMO-LUMO levels calculated using Tauc plot (UV-vis DRS) and Flat-Band Potential (Mott-Schottky) of 17M/Tp-NBD COF (yellow bar); 15M/Tp-NBD (pink bar); 12M/Tp-NBD COF (blue bar); 9M/Tp-NBD COF (green bar); 6M/Tp-NBD COF (red bar); 3M/Tp-NBD (grey bar) and 12M/Tp-NBD (ST) COF (purple bar).

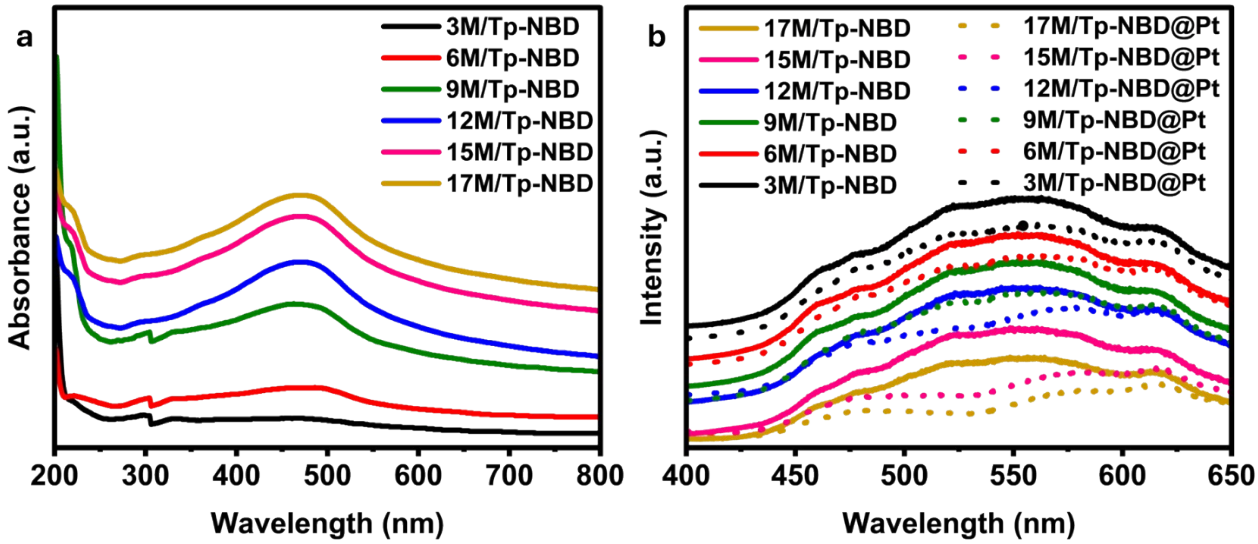

Figure S33. (a) Liquid UV and (b) Steady-state Photoluminescence spectra of 3M, 6M, 9M, 12M, 15M and 17M/Tp-NBD COFs (solid lines) and @Pt (dotted lines).

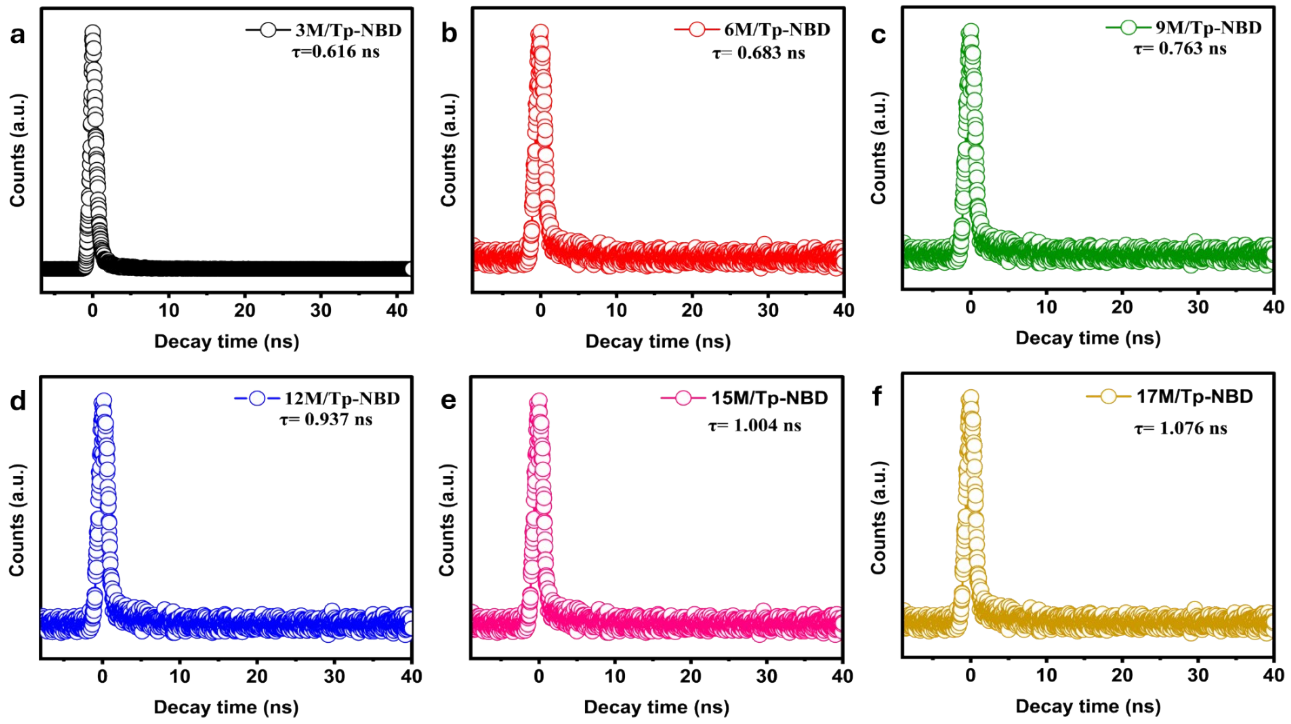

Figure S34. Time-resolved fluorescence decay spectra of (a) 3M/Tp-NBD COF; (b) 6M/Tp-NBD COF; (c) 9M/Tp-NBD COF; (d) 12M/Tp-NBD COF; (e) 15M/Tp-NBD COF; and (f) 17M/Tp-NBD COF.

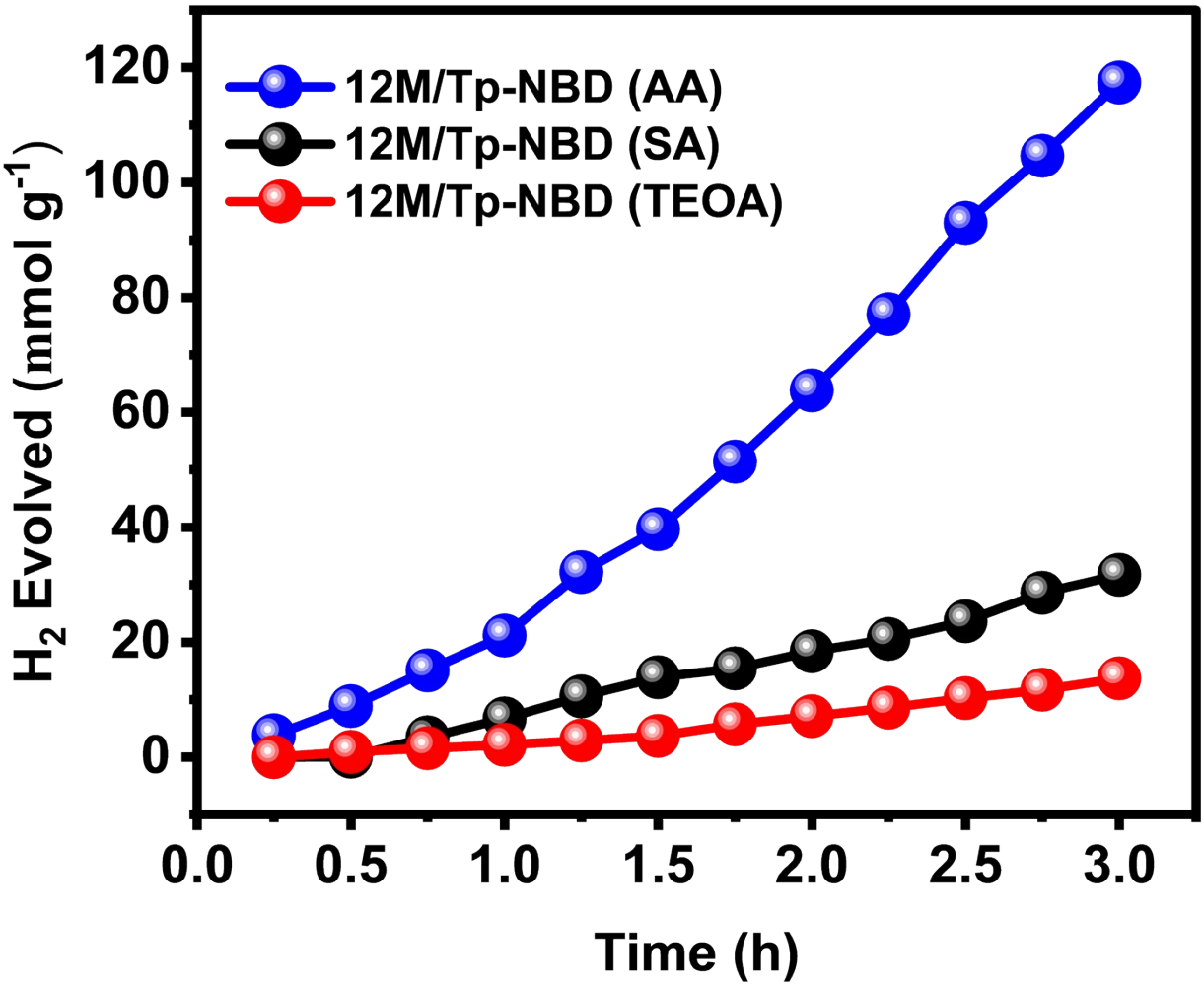

Figure S35. The photocatalytic HER activity curve of 12M/Tp-NBD COF under irradiation with AM 1.5 G light source (Xe Lamp, 300 W), 20 μL of 0.01 M H_2PtCl_6 as a source of Pt (2 wt%) using different sacrificial agents; blue curve: AA (Ascorbic Acid); black curve: SA (sodium ascorbate); red curve: TEOA (triethanolamine).

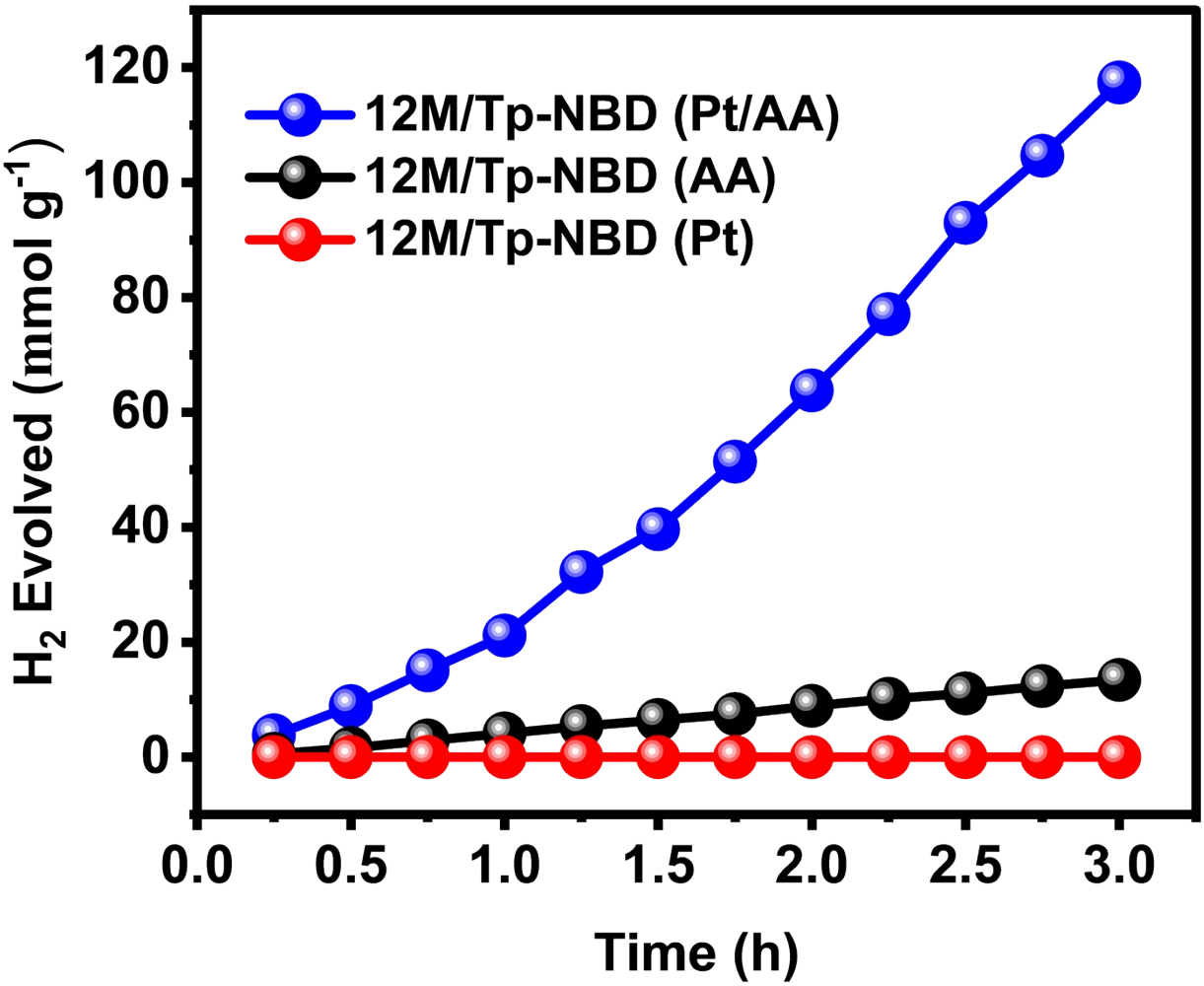

Figure S36. The photocatalytic HER activity curve of the control experiment under irradiation with AM 1.5 G light source (Xe Lamp, 300 W); (blue curve) 12M/Tp-NBD COF, 20 μL of 0.01 M H_2PtCl_6 as a source of Pt (2 wt%) and 0.05 M of Ascorbic Acid (AA); (black curve) 12M/Tp-NBD COF with 0.05 M AA; (red curve) 12M/Tp-NBD COF with 20 μL of 0.01 M H_2PtCl_6 as a source of Pt (2 wt%).

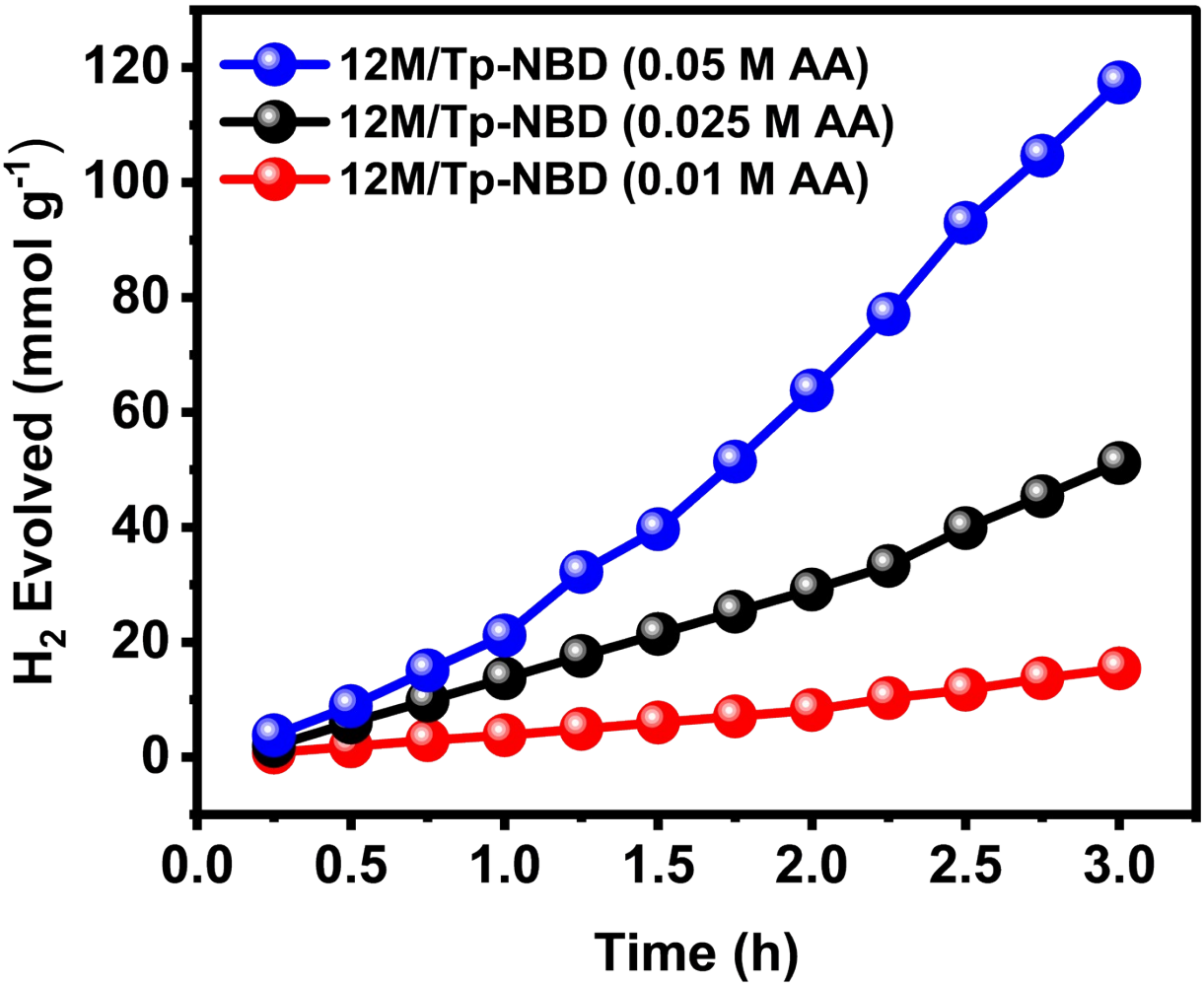

Figure S37. The photocatalytic HER activity curve of 12M/Tp-NBD COF under irradiation with AM 1.5 G light source (Xe Lamp, 300 W), 20 μL of 0.01 M H_2PtCl_6 as a source of Pt (2 wt%), with varying concentrations of AA; red curve: 0.01M AA; black curve: 0.025 M AA; blue curve: 0.05 M AA.

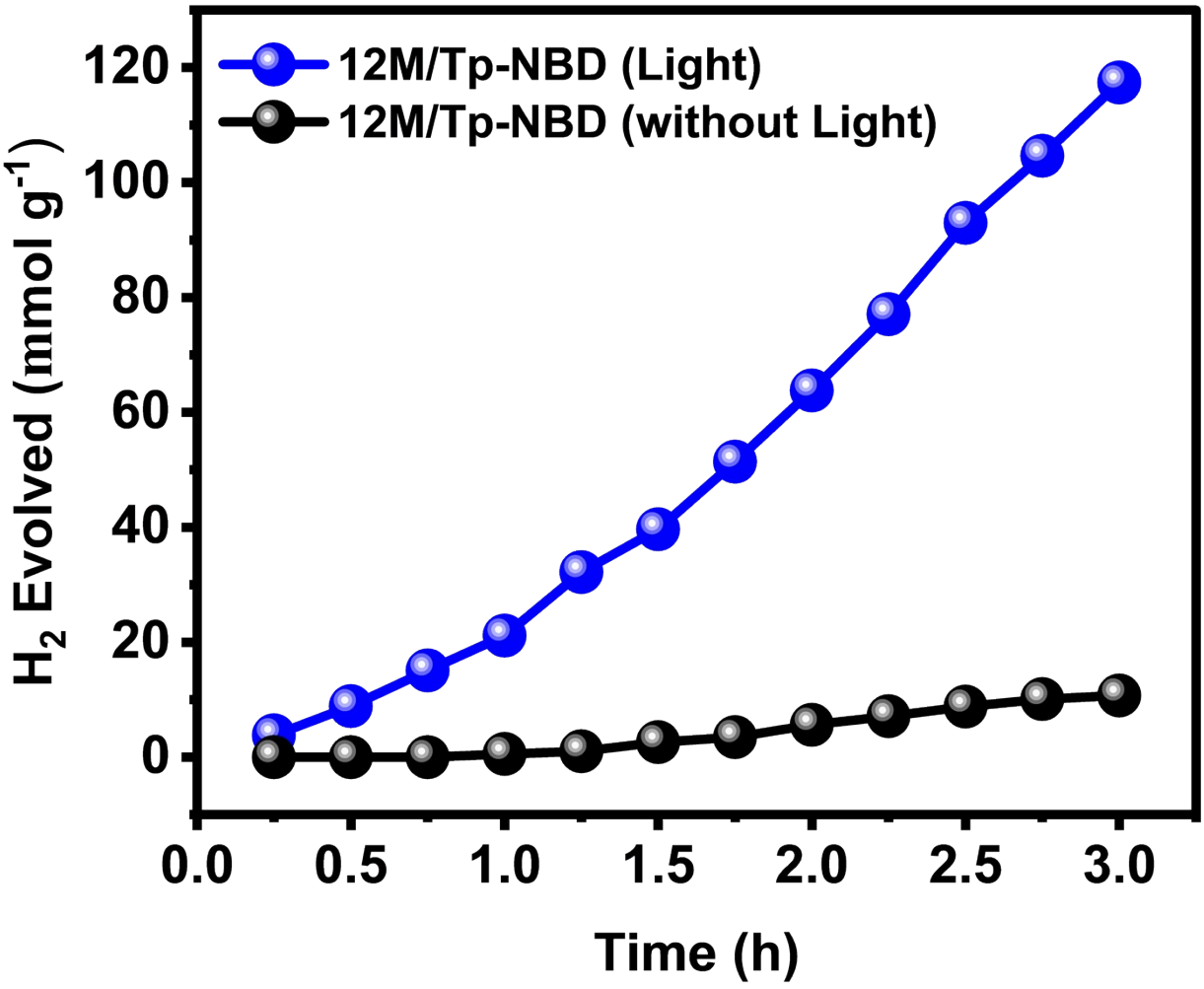

Figure S38. The photocatalytic HER curve of 12M/Tp-NBD COF, 20 μL of 0.01 M H_2PtCl_6 as a source of Pt (2 wt%) and 0.05 M of Ascorbic Acid (AA); (black curve) without light; (blue curve) under irradiation with AM 1.5 G light source (Xe Lamp, 300 W).

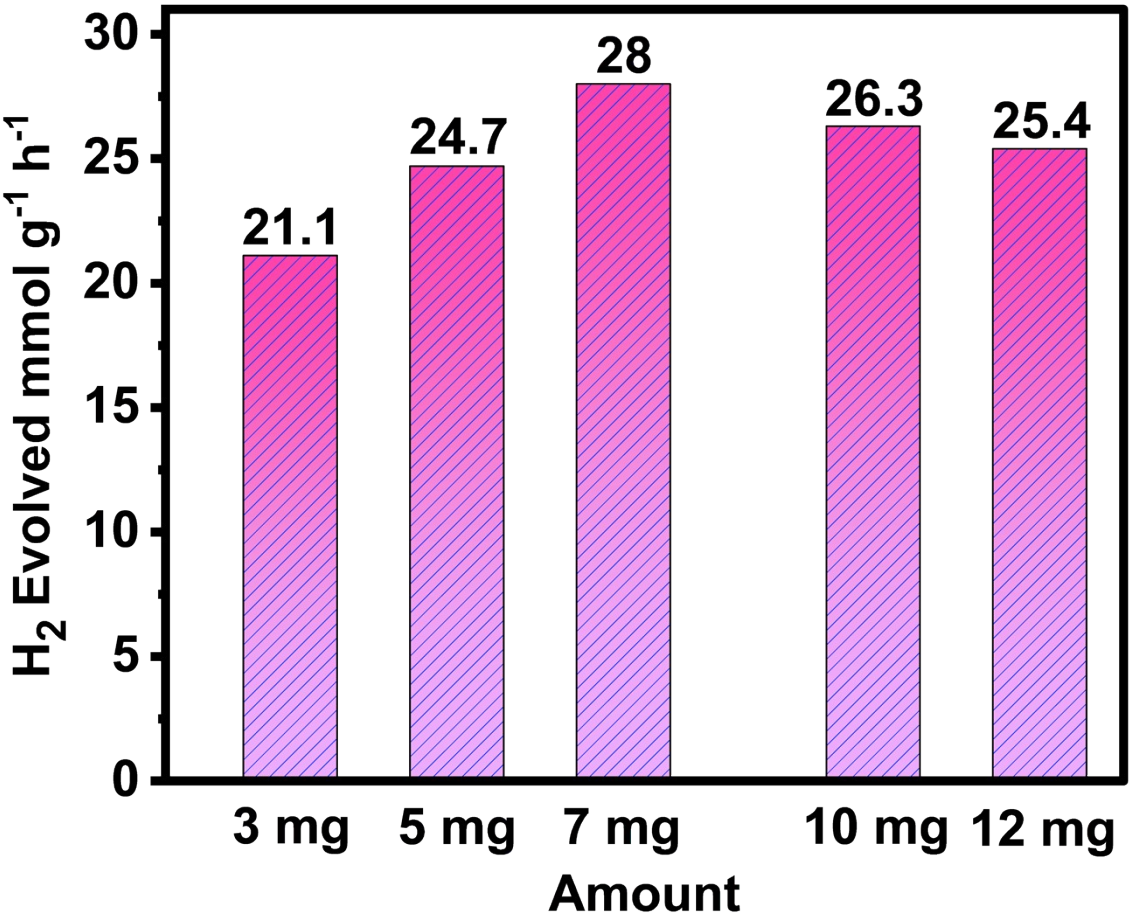

Figure S39. Rate of photocatalytic HER activity with different amounts of 12M/Tp-NBD COF under irradiation (AM 1.5 G light source, Xe Lamp, 300 W), using 20 µL of 0.01 M H_2PtCl_6 as a source of Pt (2 wt%) and 0.05 M of Ascorbic Acid (AA).

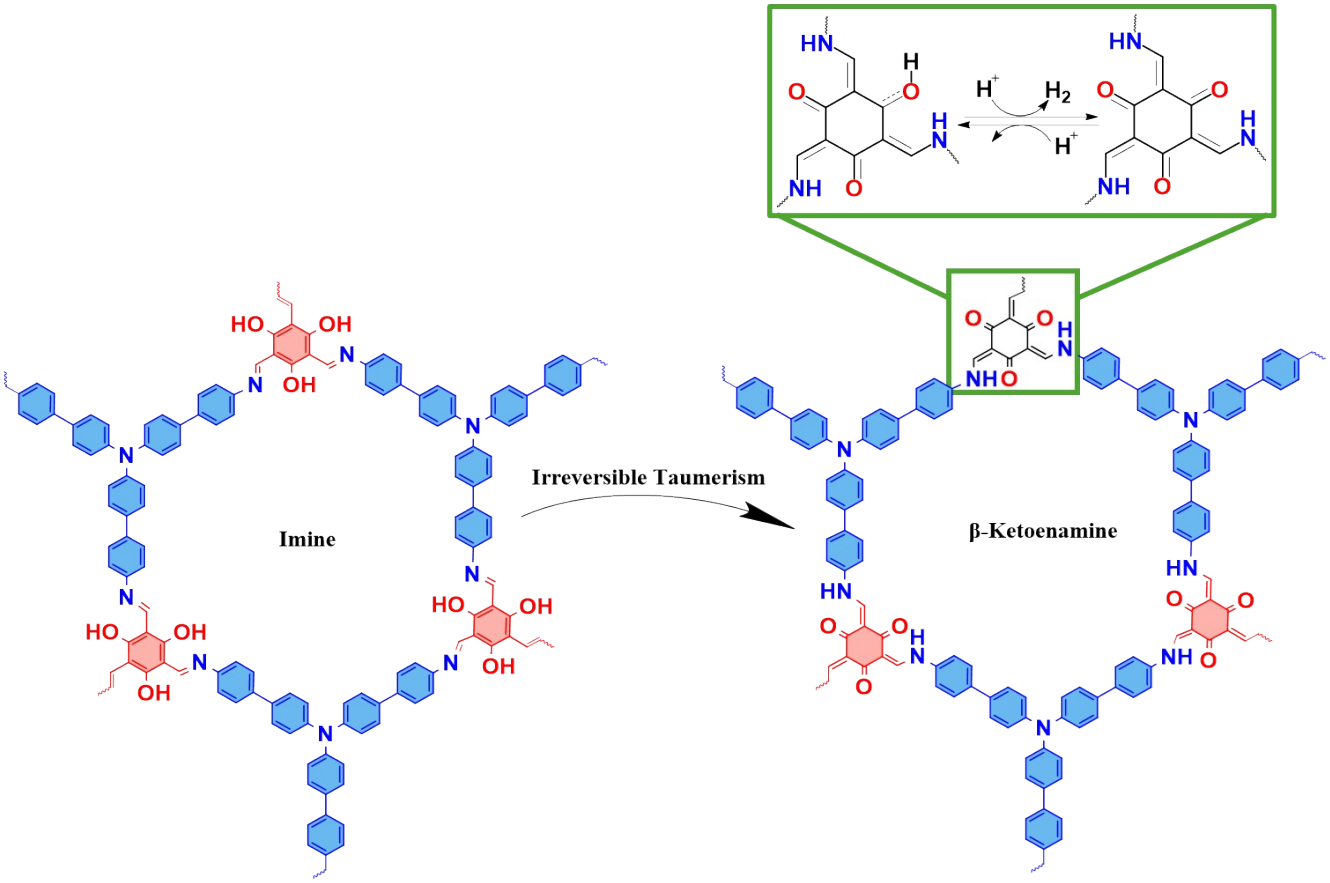

Figure S40. Irreversible Keto-Enol Tautomerism and Plausible Mechanism for HER by Tp-NBD COF.

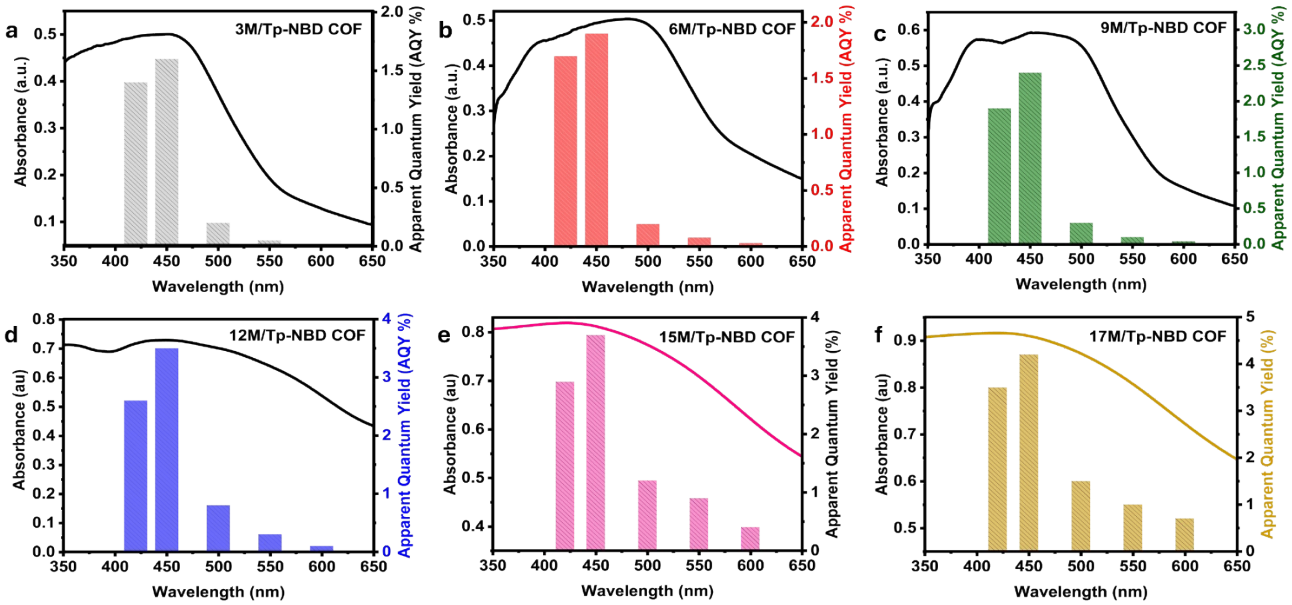

Figure S41. Absorption spectra and wavelength-specific AQYs of (a) 3M/Tp-NBD COF; (b) 6M/Tp-NBD COF; (c) 9M/Tp-NBD COF; (d) 12M/Tp-NBD COF; (e) 15M/Tp-NBD COF; and (f) 17M/Tp-NBD COF (The corresponding AQY data are summarized in Table S3).

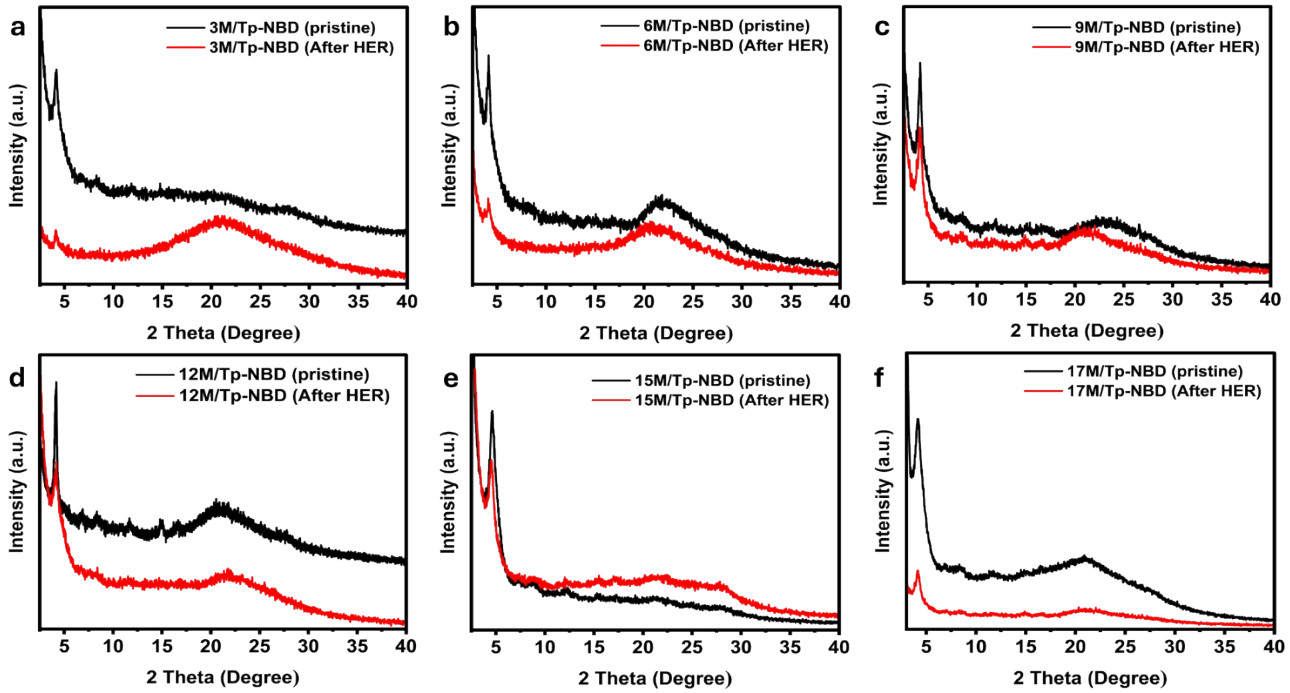

Figure S42. PXRD patterns of (a) 3M/Tp-NBD COF; (b) 6M/Tp-NBD COF; (c) 9M/Tp-NBD COF; (d) 12M/Tp-NBD COF; (e) 15M/Tp-NBD COF; and (f) 17M/Tp-NBD COF before and after photocatalytic HER activities.

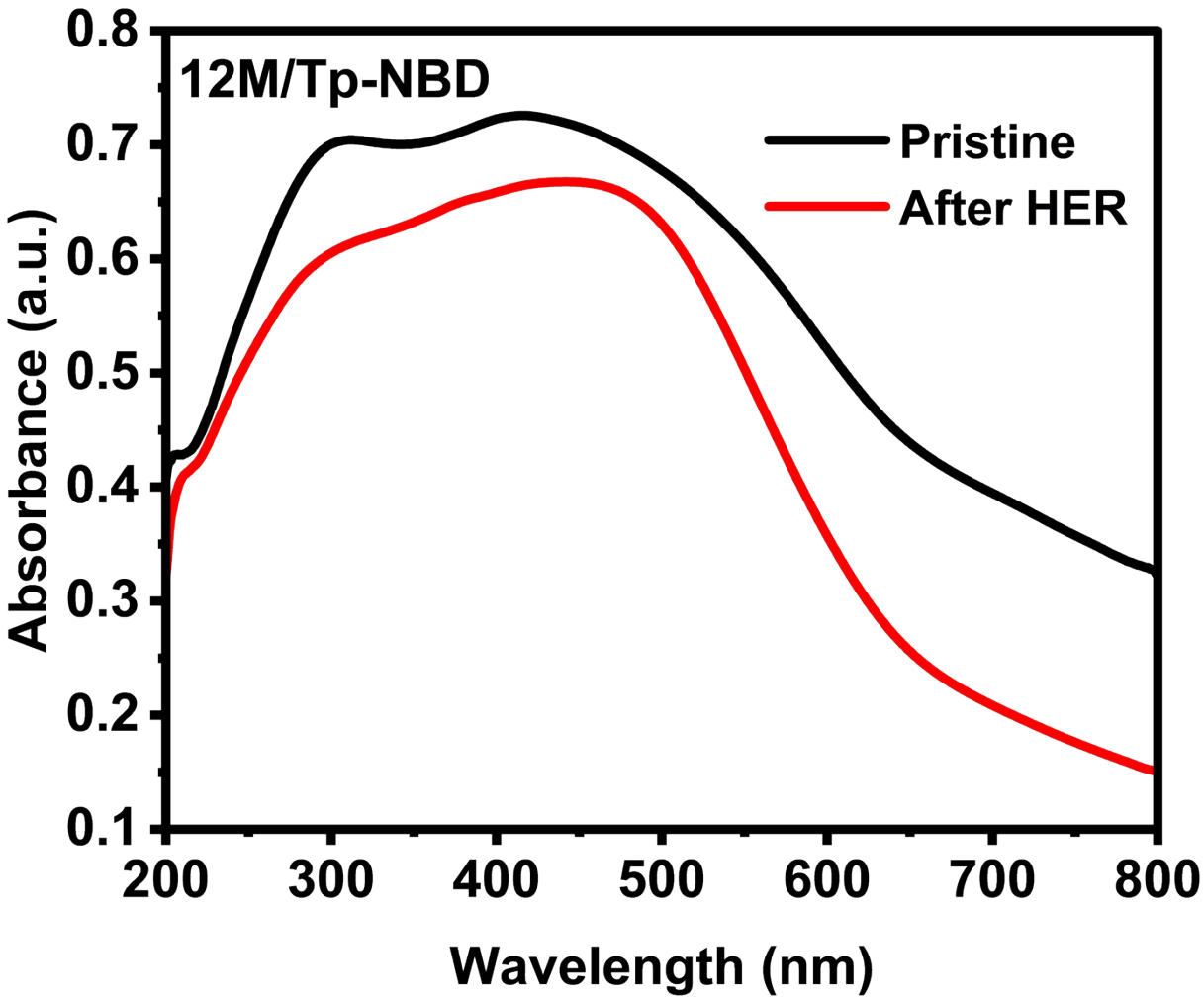

Figure S43. UV-vis DRS of 12M/Tp-NBD COF before and after photocatalytic HER activity.

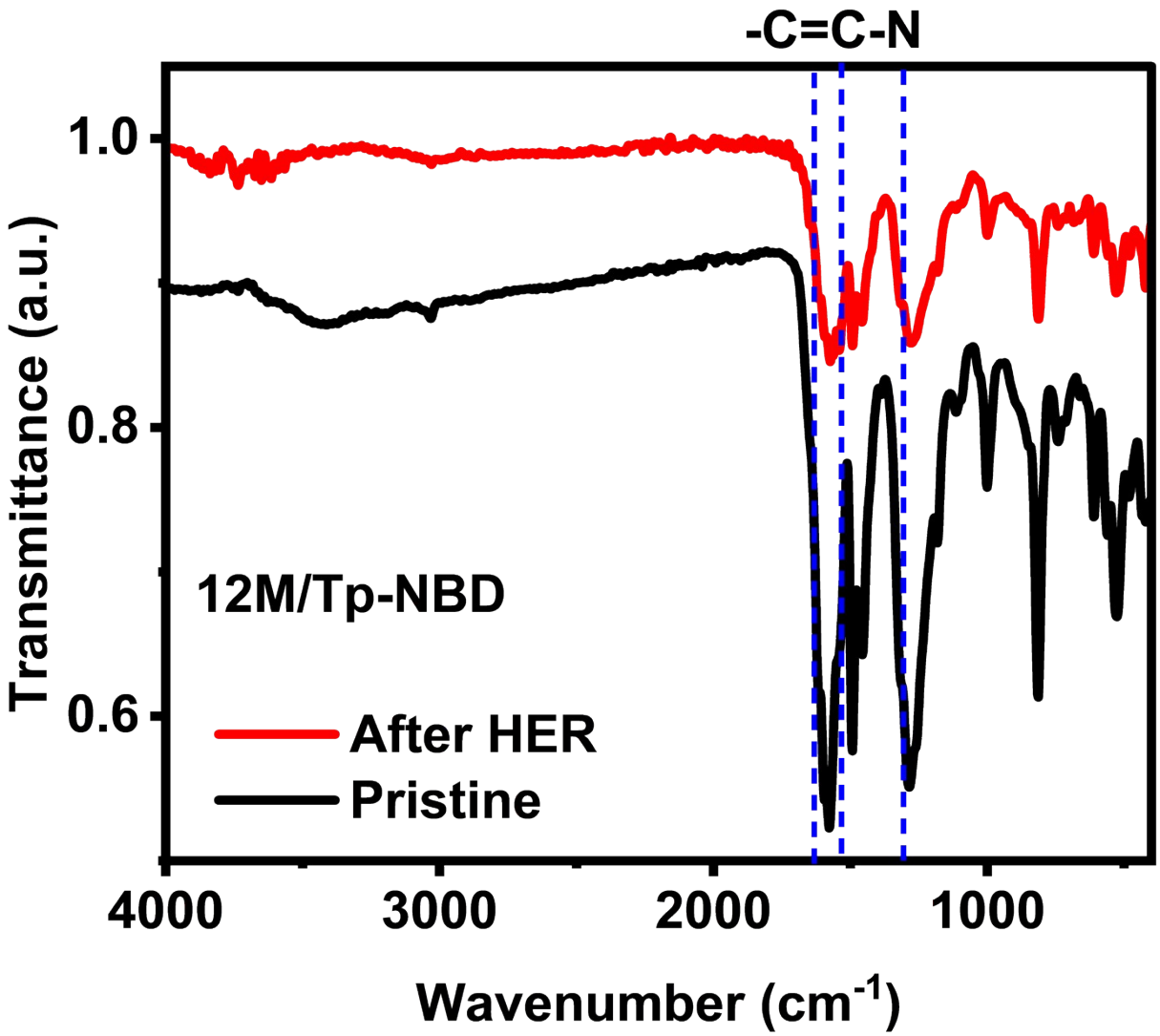

Figure S44. FT-IR spectra of 12M/Tp-NBD COF before (black curve) and after (red curve) photocatalytic HER activity.

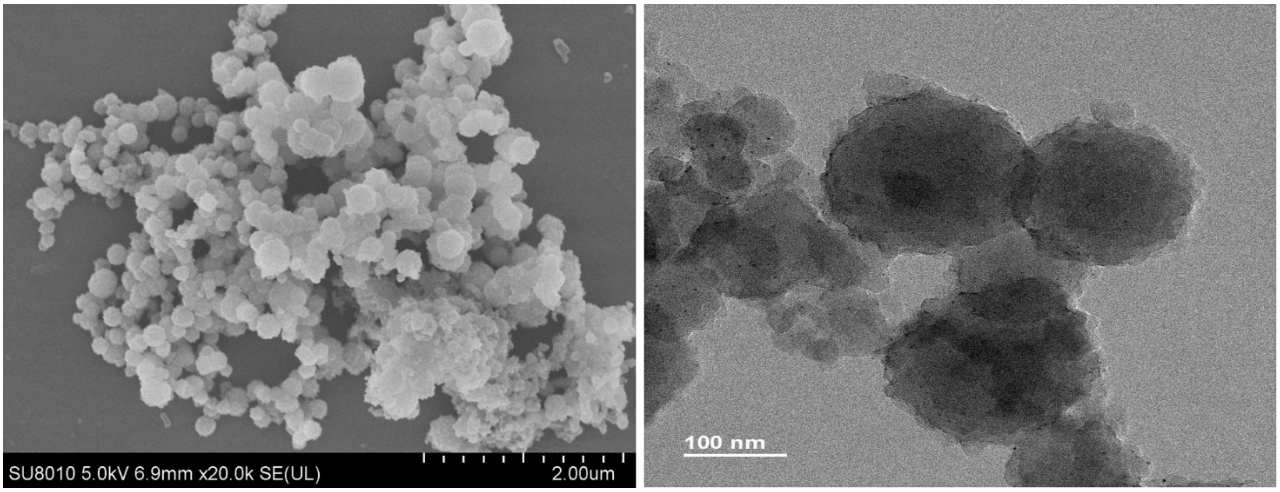

Figure S45. SEM and TEM images of 17M/Tp-NBD COF after photocatalytic HER test.

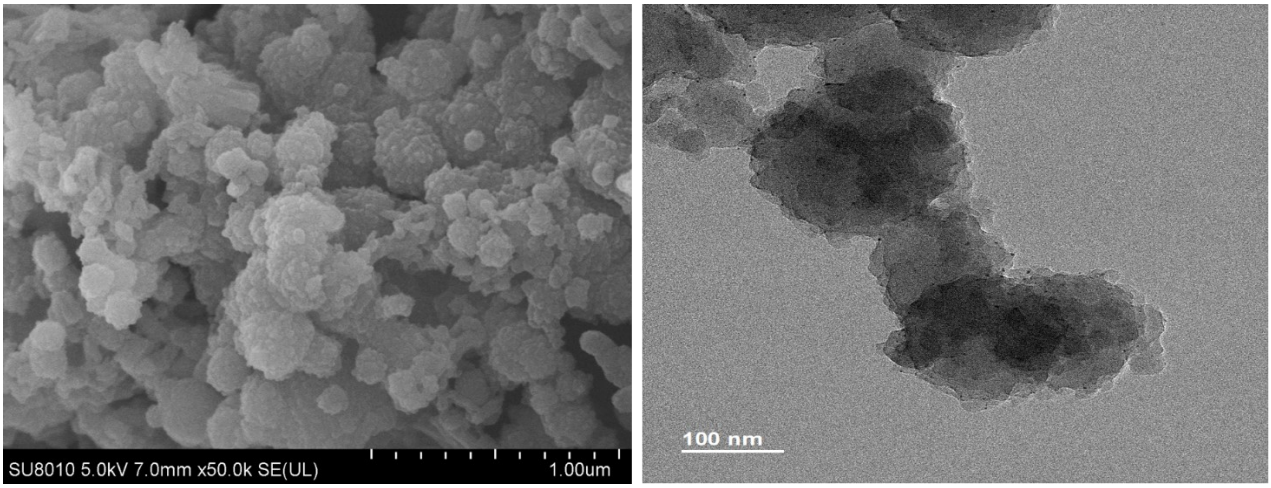

Figure S46. SEM and TEM images of 15M/Tp-NBD COF after photocatalytic HER activities.

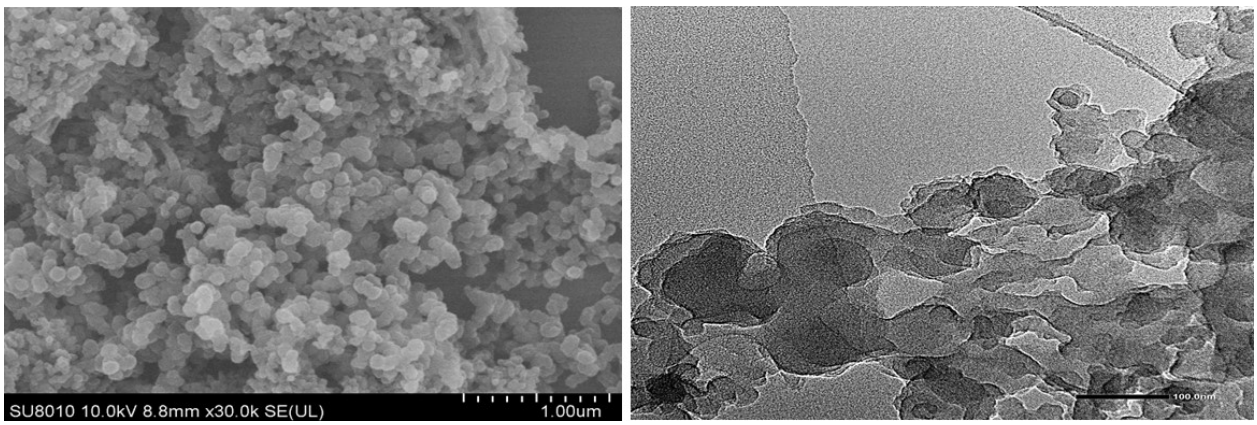

Figure S47a. SEM and TEM images of 12M/Tp-NBD COF after photocatalytic HER activities.

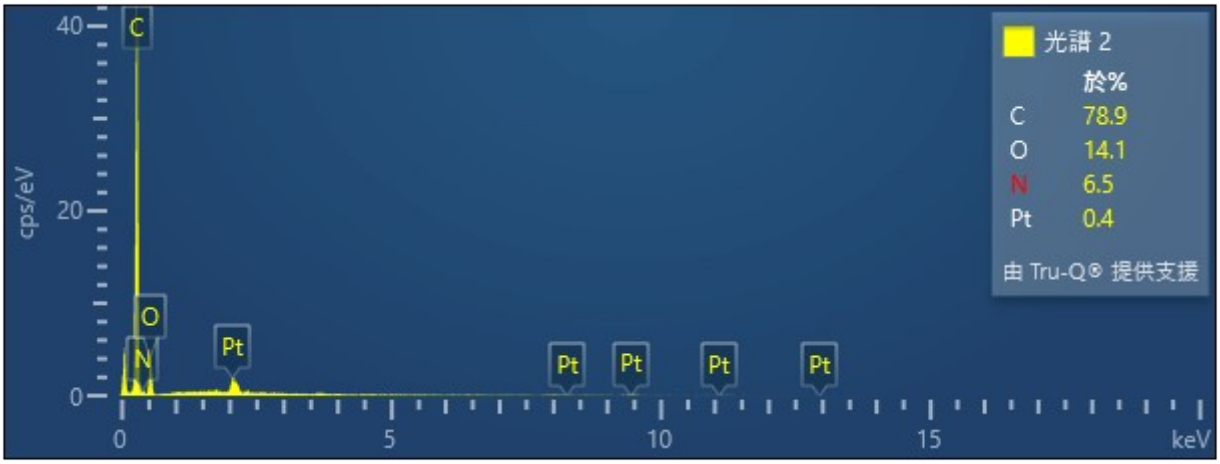

Figure S47b. EDAX Elemental Mapping image of 12M/Tp-NBD COF after photocatalytic HER test.

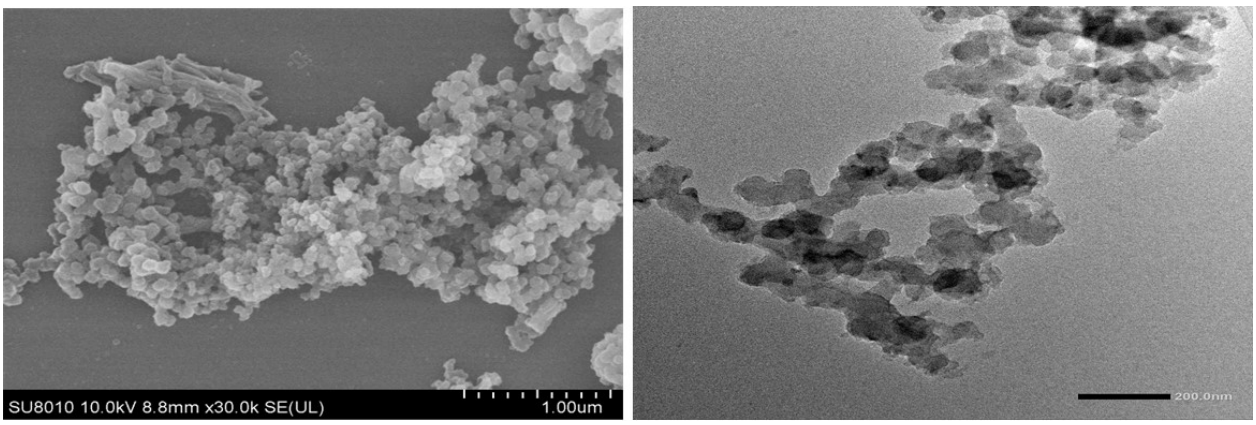

Figure S48a. SEM and TEM images of 9M/Tp-NBD COF after photocatalytic HER activities.

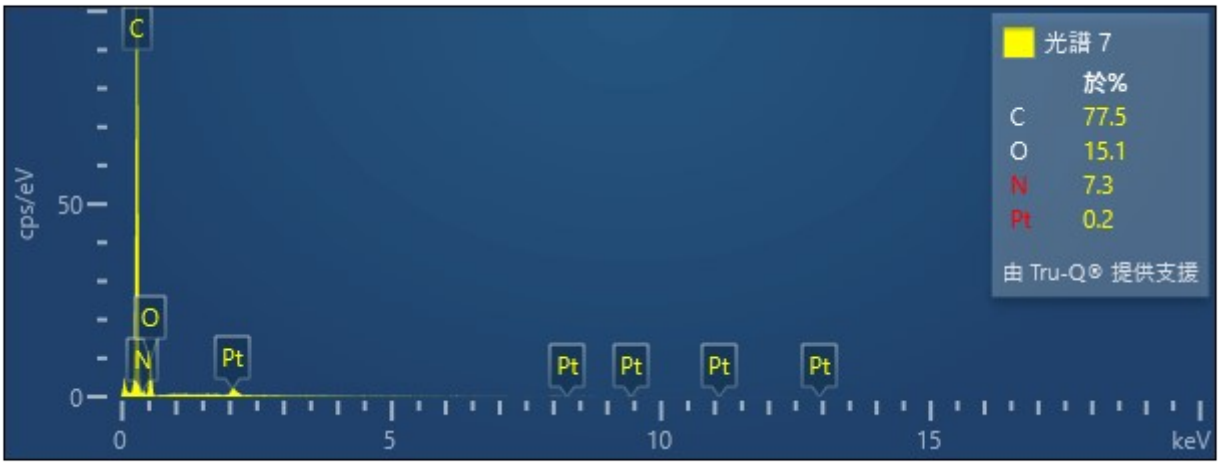

Figure S48b. EDAX Elemental Mapping image of 9M/Tp-NBD COF after photocatalytic HER test

The absence of clearly visible Pt nanoparticles in the TEM images is attributed to the low loading (2 wt%) and likely dispersion of Pt as sub-nanometric clusters. To support this, we have included EDAX elemental mapping (Figure S47b and S48b), which confirms the presence of Pt in the post-HER samples, indicating that Pt is still present on the COF surface. These results support that the absence of visible Pt particles in the TEM images is not due to leaching, but rather to the ultrafine and dispersed nature of the deposited Pt species.

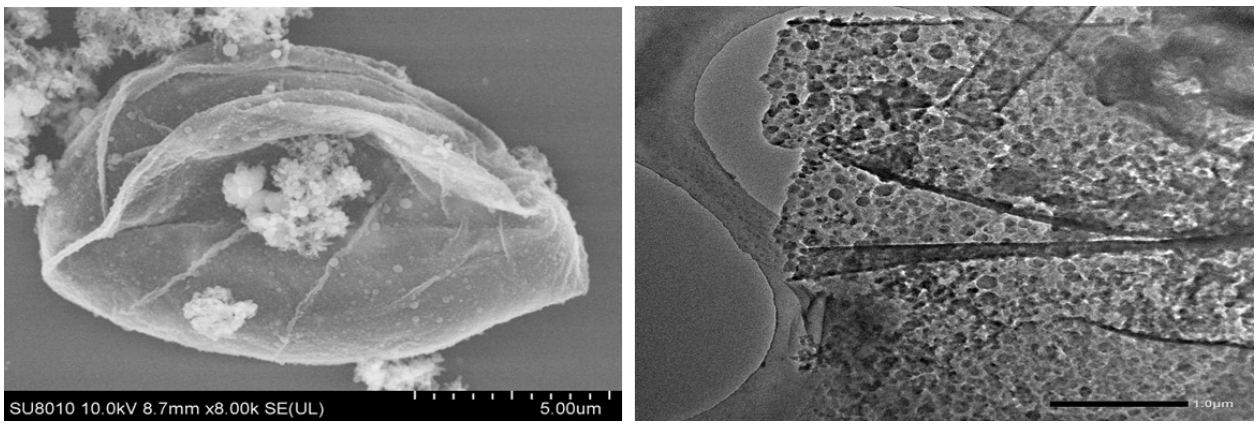

Figure S49. SEM and TEM images of 6M/Tp-NBD COF after photocatalytic HER activities.

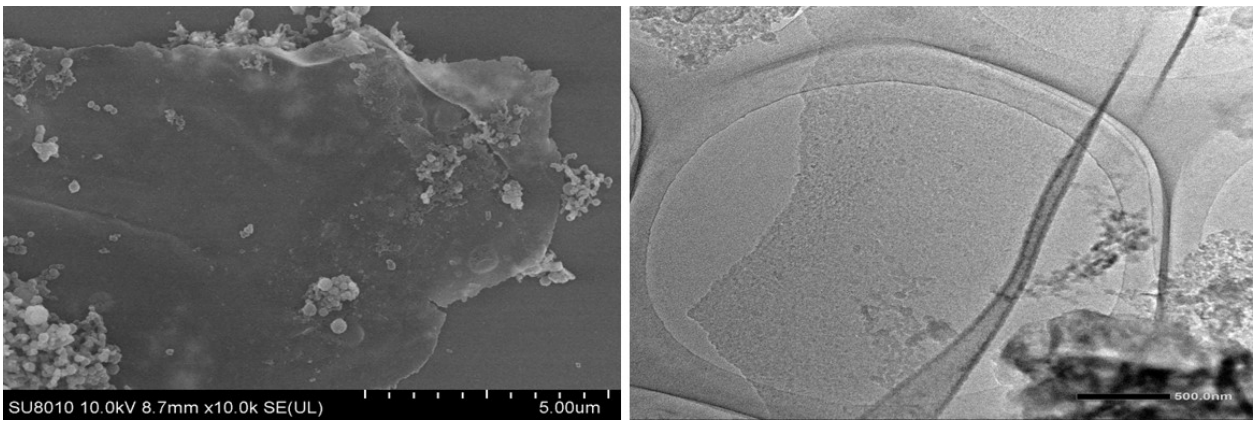

Figure S50. SEM and TEM images of 3M/Tp-NBD COF after photocatalytic HER activities.

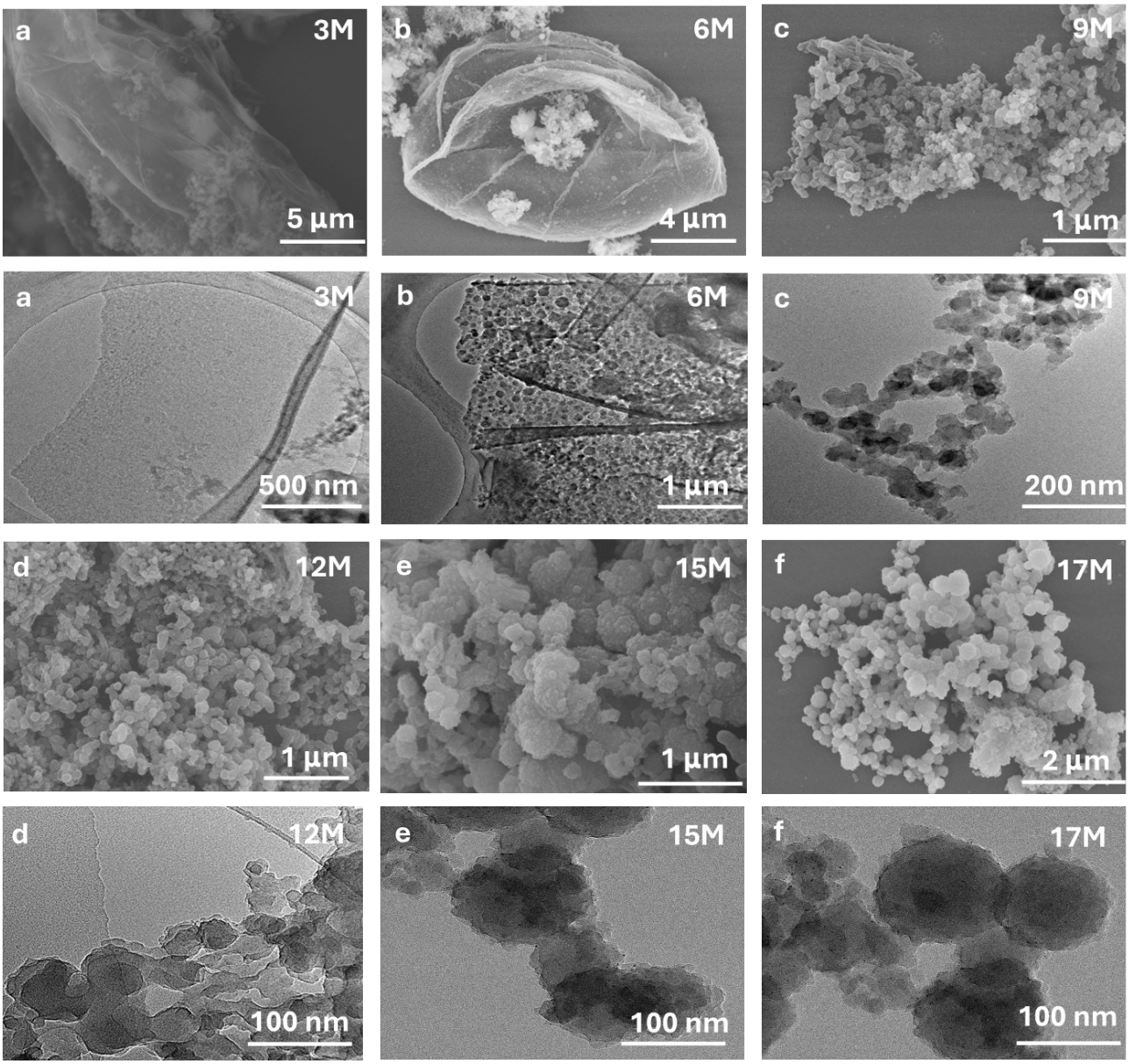

Figure S51. SEM and TEM images of (a) 3M/Tp-NBD; (b) 6M/Tp-NBD; (c) 9M/Tp-NBD; (d) 12M/Tp-NBD; (e) 15M/Tp-NBD; and (f) 17M/Tp-NBD COFs after photocatalytic HER activities for comparison of morphologies.

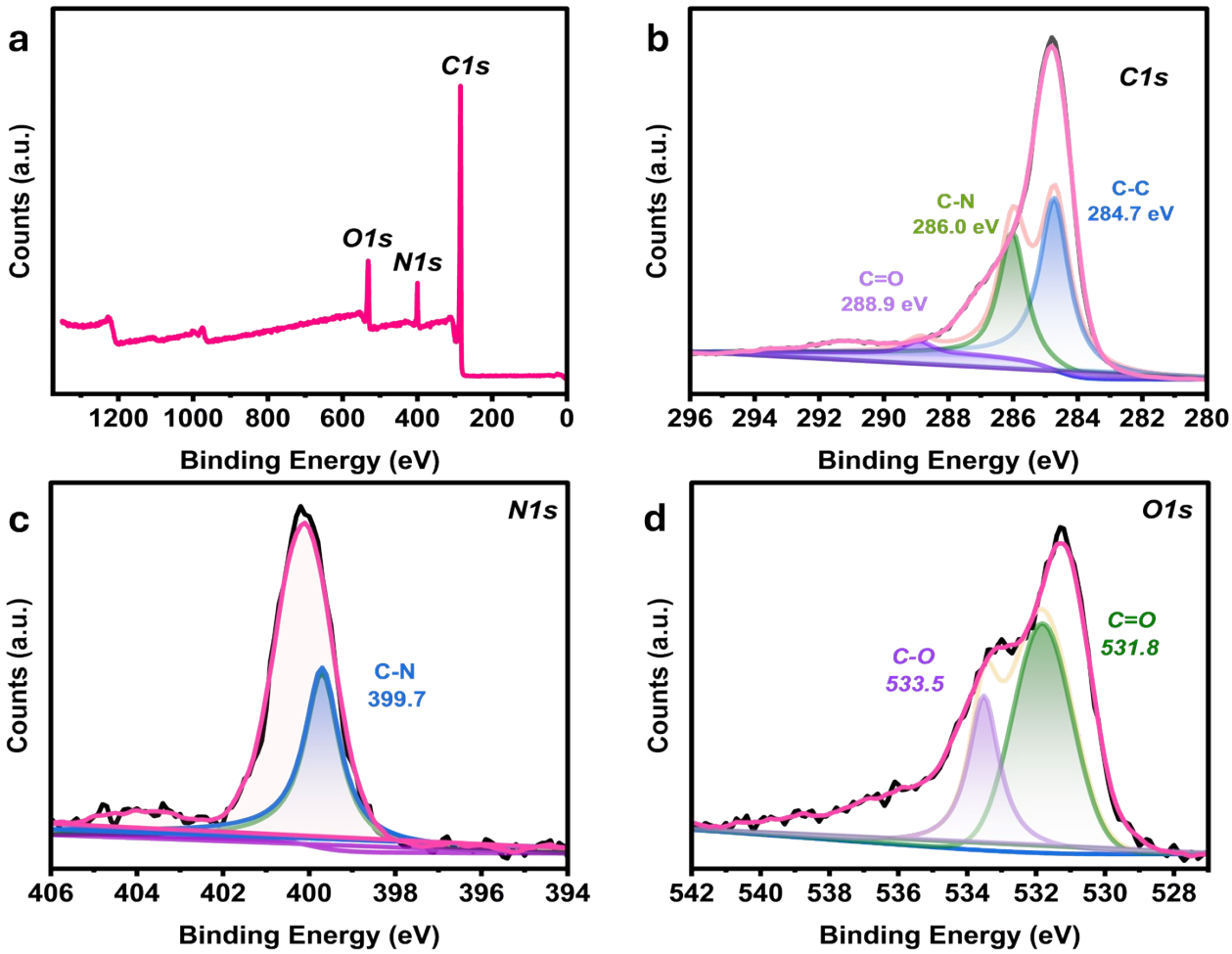

Figure S52. (a) XPS survey; and High-Resolution XPS spectra of (b) C1s; (c) N1s; and (d) O1s scans of 12M/Tp-NBD COF after HER activities.

Table S1. Structural Properties of 3-17M/Tp-NBD and 12M/Tp-NBD (ST) COFs obtained from N_2 Adsorption Desorption Isotherm

COF	*S BET (m^2 g^{-1})	** V total (cm^3 g^{-1}) (P/P_0= 0.999)	Pore size (nm)
3M/Tp-NBD	63.4	0.11	6.9
6M/Tp-NBD	311.5	0.31	3.9
9M/Tp-NBD	391.6	0.41	4.2
12M/Tp-NBD	677.5	0.47	2.8
15M/Tp-NBD	893.2	0.66	2.7
17M/Tp-NBD	1058.6	0.84	3.2
12M/Tp-NBD (ST)	456	0.35	3.1

* BET Surface area. ** Total pore volume.

Table S2. Optoelectronic band gap calculated from UV-vis DRS and Mott Schottky for 3-17M/Tp-NBD and 12M/Tp-NBD (ST) COFs

COF Name	Optical Band Gap (eV)	Mott Schottky (E_{fb}) V vs NHE	HOMO V vs NHE
3M/Tp-NBD	1.84	-1.09	0.75
6M/Tp-NBD	1.83	-1.1	0.73
9M/Tp-NBD	1.85	-1.14	0.71
12M/Tp-NBD	1.83	-1.16	0.67
15M/Tp-NBD	1.82	-1.15	0.67
17M/Tp-NBD	1.81	-1.12	0.69
12M/Tp-NBD (ST)	1.83	-0.46	1.37

Table S3. Apparent Quantum Yield (AQY %) at different wavelengths of 3-17M/Tp-NBD COFs

COF Sample	AQY (%) 420 nm	AQY (%) 450 nm	AQY (%) 500 nm	AQY (%) 550 nm	AQY (%) 600 nm
3M/Tp-NBD	1.4	1.6	0.2	0.05	0.02
6M/Tp-NBD	1.7	1.9	0.2	0.08	0.03
9M/Tp-NBD	1.9	2.4	0.3	0.1	0.04
12M/Tp-NBD	2.6	3.5	0.8	0.3	0.1
15M/Tp-NBD	2.9	3.7	1.2	0.9	0.4
17M/Tp-NBD	3.5	4.2	1.5	1	0.7

Table S4: Periodic Comparison of the rate of Photocatalytic HER activities of pristine Tp-COFs with the current study

Tp-COFs	Cocatalyst	Sacrificial Agent	Light Source	HER *(mmol g^{-1} h^{-1})	Year	Ref.
Tp-COF	Pt	LA	400 W, Xe $\lambda \geq 420$ nm	0.028	2014	6
EB-COF	-	AA	300 W, Xe $\lambda \geq 420$ nm	1.57	2018	7
TP-COF	Pt	AA	300 W, Xe $\lambda > 420$ nm	1.6	2018	8
S-COF	Pt	AA	300 W, Xe $\lambda > 420$ nm	4.44		
FS-COF	Pt	AA	300 W, Xe $\lambda > 420$ nm	10.1		
TpPa-1-COF	Pt	SA	300 W, Xe $\lambda = 420$ nm	1.22	2018	9
TpDTz COF	NiME	TEOA	300 W, Xe AM 1.5	0.941	2019	10
TpPa-COF	Pt	SA	300 W Xe $\lambda = 420$ nm	1.56	2019	11
TpPa-COF-$(CH_3)_2$	Pt	SA	300 W Xe $\lambda = 420$ nm	8.33		
Tppa-COF-NO_2	Pt	SA	300 W Xe $\lambda = 420$ nm	0.22		
TpPa-2	-	SA	300W Xe, $\lambda = 420$ nm	0.07209	2020	12
TPPA	Pt	SA	300 W, Xe $\lambda > 420$ nm	0.002384	2020	13
TBTA-COF	-	AA	300 W, Xe $\lambda \geq 420$ nm	2.47	2021	14
Tp-DBN	Pt	SA	300 W, Xe $\lambda > 420$ nm	1.8	2021	15
Tp(BT_xTP_{1-x})-COF	Pt	AA	300 W, Xe $\lambda = 420$ nm	9.839	2021	16
CYANO-COF	Pt	AA	300 W, Xe $\lambda > 420$ nm	1.217	2022	17
Tz-COF-3	Pt	0.8 M AA	300 W, Xe $\lambda > 420$ nm	43.2	2022	18
Tp-Pa-2	$Cu_3(HHTP)_2$	SA	300 W Xe, $\lambda = 400$ nm	7.71	2022	19
TpBD-COF	NiS	Na_2S/Na_2SO_3	300 W, Xe $\lambda > 420$ nm	3.840	2022	20
TP-COF	PVP-Pt	SA	300 W, Xe $\lambda > 420$ nm	8.6	2022	21
TpPa-1-COF	-	Na_2S/Na_2SO_3	$\lambda \geq 420$ nm	0.137	2023	22
TpTAP-COF	Pt	AA	300 W, Xe $\lambda > 420$nm	13.5	2023	23
COF-H	Pt	AA	AM 1.5 G	5.03	2023	24
Tp-DB-$(OCH_3)_2$-COF	Pt	PBS	300 W Xe, $\lambda = 400$ nm	1.23	2023	25
Tp-DB-$(CH_3)_2$-COF	Pt	PBS	300 W Xe, $\lambda = 400$ nm	0.81		
Tp-DB-COF	Pt	PBS	300 W Xe, $\lambda = 400$ nm	0.60		
Tp-DB-$(NO_2)_2$-COF	Pt	PBS	300 W Xe, $\lambda = 400$ nm	0.015		
BT-COF-2	Pt	AA	300 W, Xe $\lambda > 420$nm	12.58	2024	26
BT-COF-3	Pt	AA	300 W, Xe $\lambda > 420$nm	2.07		

Tp-Tta COF	Co	TEOA	300 W Xe, λ > 320 nm	1.7985	2024	[27]
CH_3I-TpPa-1	-	AA	300 W, Xe λ > 420nm	9.21	2024	[28]
CH_3I-TpBD	-	AA	300 W, Xe λ > 420nm	4.72		
CH_3I-TpEDDA	-	AA	300 W, Xe λ > 420nm	2.96		
CH_3I-TpBpy	-	AA	300 W, Xe λ > 420nm	2.39		
CH_3I-TpAzo	-	AA	300 W, Xe λ > 420nm	5.64		
S-COF	Pt/ IrO_2 (OWS)	AA	300 W, Xe λ > 420 nm	0.0566	2024	[29]
DS-COF	Pt/ IrO_2 (OWS)	AA	300 W, Xe λ > 420 nm	0.124		
TS-COF	Pt/ IrO_2 (OWS)	AA	300 W, Xe λ > 420 nm	0.03		
3M/Tp-NBD	Pt	AA	300 W, Xe (AM 1.5 G)	9.7	2025	This work
6M/Tp-NBD	Pt	AA	300 W, Xe (AM 1.5 G)	14.1		
9M/Tp-NBD	Pt	AA	300 W, Xe (AM 1.5 G)	16		
12M/Tp-NBD	Pt	AA	300 W, Xe (AM 1.5 G)	21.1		
15M/Tp-NBD	Pt	AA	300 W, Xe (AM 1.5 G)	25.5		
17M/Tp-NBD	Pt	AA	300 W, Xe (AM 1.5 G)	32.7		
12M/Tp-NBD-ST	Pt	AA	300 W, Xe (AM 1.5 G)	0.861		

AA = Ascorbic Acid, LA = Lactic Acid, SA = Sodium Ascorbate, TEOA = Triethanolamine, NiME = Ni-thiolate-2-mercaptoethanol, OWS = overall water splitting

* Values are reported in mmol g^{-1} h^{-1} for convenience

Table S5: Periodic Comparison of the rate of Photocatalytic HER activities of hybrid/hetero-Tp-COFs

Tp-COFs	Cocatalyst	Sacrificial Agent	Light Source	HER *(mmol g^{-1} h^{-1})	Year	Ref
CdS-COF	Pt	LA	400 W, Xe $\lambda \geq 420$ nm	3.6	2014	6
Mo_3S_{13}@EB-COF	$Ru(bpy)_3Cl_2$	AA	300 W, Xe $\lambda \geq 420$ nm	13.2	2018	7
NH_2-UiO-66/TpPa-1-COF	Pt	SA	300 W, Xe $\lambda = 420$ nm	1.22	2018	9
MoS_2/TpPa-1-COF	-	AA	300 W, Xe $\lambda > 420$ nm	5.58	2019	30
TiO_2-TpPa-1-COF	Pt	SA	300 W, Xe $\lambda = 420$ nm	11.19	2020	31
CNS-TTA-TP-COF	Pt	TEOA	300 W, Xe $\lambda > 420$ nm	46.4	2020	32
rGO-TpPa-1-COF	Pt	SA	300 W, Xe $\lambda = 420$ nm	11.98	2020	33
αFe_2O_3/TpPa-2-COF	-	SA (PBS)	300 W, Xe $\lambda \geq 420$ nm	3.77	2020	34
CdS@TPPA	Pt	SA	300 W, Xe $\lambda = 420$ nm	24.3	2021	12
MOF-808@TpPa-1-COF	Pt	SA	300 W, Xe $\lambda = 420$ nm	11.88	2021	35
PEG@BT-COF	Pt	AA	300 W, Xe $\lambda > 420$ nm	11.14	2021	36
TpPa-1 COF/g-C_3N_4	Pt	SA (PBS)	300 W, Xe $\lambda \geq 420$ nm	1.153	2022	37
Cu-NH_2-MIL-125/TpPa-2-COF	-	SA (PBS)	300 W, Xe $\lambda > 420$ nm	9.21	2022	38
WO_3@TpPa-1-COF/rGO	Pt	SA	300 W, Xe $\lambda > 420$ nm	26.73	2022	39
Pt/rGO/TpPa-1-COF	Pt	SA	300 W, Xe $\lambda > 420$ nm	10.22	2022	40
MX/TPNCOF@ZIS	-	AA	300 W, Xe $\lambda \geq 420$ nm	4.01	2023	41
PABZ-Tp	Pt	AA	300 W, Xe $\lambda > 420$ nm	115	2023	42
TSCOFW	Pt	AA	300 W, Xe $\lambda > 420$ nm	539	2023	43
FOOPh-COF	Pt	AA	350 W, Xe $\lambda > 420$ nm	228.5	2024	44
$CuCo_2O_4$/TpPaCOF	-	AA	300 W, Xe $\lambda \geq 420$ nm	8.3	2024	45
TpBP-CN COF	Pt	AA	300 W, Xe $\lambda \geq 420$ nm	162.7	2024	46
TpPa-Cl_2	Pt	AA	300 W, Xe $\lambda \geq 420$ nm	99.23	2024	47
TpPa-CN_2	Pt	AA	300 W, Xe $\lambda \geq 420$ nm	76.93		
TiN@TFP-BD	Pt	SA	300 W, Xe $\lambda > 420$ nm	37.59	2024	48
TFP-BpyD nano-COF	Pt	AA	1440 W, Xe AM 1.5 G	392	2024	49
TFP-BD nano-COF	Pt	AA	1440 W, Xe AM 1.5 G	183		
TpPa-SCOF-An	Pt	AA	300 W, Xe $\lambda > 420$ nm	126	2025	50
SiO_2@TpPa-An	Pt	AA	300 W, Xe $\lambda > 420$ nm	350		

References

1 Y. Li, Q. Wu, X. Guo, M. Zhang, B. Chen, G. Wei, X. Li, X. Li, S. Li, L. Ma, *Nat. Commun.,* 2020, **11**, 599.

2 P. Pachfule, O. Acharjya, J. Roeser, T. Langenhahn, M. Schwarze, R. Schomäcker, A. Thomas, O. Schmidt, *J. Am. Chem. Soc.,* 2018, **140**, 1423–1427.

3 Y. Wang, Z. Qiao, H. Li, R. Zhang, Z. Xiang, D. Cao, S. Wang, *Angew. Chem. Int. Ed. Engl.,* 2024, **63**, e202404726.

4 M. Ran, X. Zhang, J. Lin, R. A. Borse, L. Zhang, Y. Wang, *J. Mater. Chem. A,* 2025, **13**, 1123–1134;

5 Z. Mi, T. Zhou, W. Weng, J. Unruangsri, K. Hu, W. Yang, C. Wang, K. A. I. Zhang, J. Guo, *Angew. Chem. Int. Ed. Engl.,* 2021, **60**, 9642–9649.

6 J. Thote, H. B. Aiyappa, A. Deshpande, D. Diaz Diaz, S. Kurungot, R. Banerjee, *Chem. Eur. J.,* 2014, **20**, 15961–15965.

7 Y. J. Cheng, R. Wang, S. Wang, X. J. Xi, L. F. Ma, S. Q. Zang, *Chem. Commun.,* 2018, **54**, 13563–13566.

8 X. Wang, L. Chen, S. Y. Chong, M. A. Little, Y. Wu, W. H. Zhu, R. Clowes, Y. Yan, M. A. Zwijnenburg, R. S. Sprick, A. I. Cooper, *Nat. Chem.,* 2018, **10**, 1180–1189.

9 F. M. Zhang, J. L. Sheng, Z. D. Yang, X. J. Sun, H. L. Tang, M. Lu, H. Dong, F. C. Shen, J. Liu, Y. Q. Lan, *Angew. Chem. Int. Ed. Engl.,* 2018, **57**, 12106–12110.

10 J. L. Sheng, H. Dong, X. B. Meng, H. L. Tang, Y. H. Yao, D. Q. Liu, L. L. Bai, F. M. Zhang, J. Z. Wei, X. J. Sun, *ChemCatChem.,* 2019, **11**, 2313–2319.

11 H. Dong, X.-B. Meng, X. Zhang, H.-L. Tang, J.-W. Liu, J.-H. Wang, J.-Z. Wei, F.-M. Zhang, L.-L. Bai, X.-J. Sun, *Chem. Eng. J.,* 2020, **379**, 122368.

12 Y. Chen, D. Yang, Y. Gao, R. Li, K. An, W. Wang, Z. Zhao, X. Xin, H. Ren, Z. Jiang, *Res.,* 2021, **2021**, 9798564.

13 C. Lin, C. Han, L. Gong, X. Chen, J. Deng, D. Qi, Y. Bian, K. Wang, J. Jiang, *Catal. Sci. Technol.,* 2021, **11**, 2616–2621.

14 L. Wang, L. Zhang, B. Lin, Y. Zheng, J. Chen, Y. Zheng, B. Gao, J. Long, Y. Chen, *Small,* 2021, **17**, 2101017.

15 T. Zhou, X. Huang, Z. Mi, Y. Zhu, R. Wang, C. Wang, J. Guo, *Polym. Chem.,* 2021, **12**, 3250–3256.

16 C. Li, J. Liu, H. Li, K. Wu, J. Wang, Q. Yang, *Nat. Commun.,* 2022, **13**, 2357.

17 F. Liu, Y. He, X. Liu, Z. Wang, H.-L. Liu, X. Zhu, C.-C. Hou, Y. Weng, Q. Zhang, Y. Chen, *ACS Catal.* 2022, **12**, 9494–9502.

18 P. Xue, X. Pan, T. Tian, M. Tang, W. Guo, J. Li, Z. Wang, H. Tang, *Catal. Sci. Technol.,* 2022, **12**, 3158–3164.

19 Y. H. Yao, Y. Yang, Y. Wang, H. Zhang, H. L. Tang, H. Y. Zhang, G. Zhang, Y. Wang, F. M. Zhang, H. Yan, *J. Colloid Interface Sci.,* 2022, **608**, 2613–2622.

20 W. Zhang, S. Wang, N. Wen, J. Zhao, W. Guo, S. Wu, P. Zhang, Q. Lin, J. Xu, J. Long, *Mater. Today Chem.,* 2022, **26**, 101125.

21 P. Dong, T. Cheng, J.-L. Zhang, J. Jiang, L. Zhang, X. Xi, J. Zhang, *ACS Appl. Energy Mater.,* 2023, **6**, 1103–1115.

22 R. Gao, J. Bai, R. Shen, L. Hao, C. Huang, L. Wang, G. Liang, P. Zhang, X. Li, *J. Mater. Sci. Technol.,* 2023, **137**, 223–231.

23 M. Wang, Z. Wang, M. Shan, J. Wang, Z. Qiu, J. Song, Z. Li, *Chem. Mater.,* 2023, **35**, 5368–5377.

24 P. Xue, W. Chen, M. Tang, Z. Wang, Z. Wang, *Mol. Catal.,* 2023, **535**, 112924..

25 Z. Lin, S. Liu, W. Weng, C. Wang, J. Guo, *Small,* 2024, **20**, 2307138.

26 Y. Wang, A. Pan, Y. Ma, H. Du, *Int. J. Hydrogen Ener.,* 2024, **72**, 1298–1307.

27 J. Zhang, X. Li, H. Hu, H. Huang, H. Li, X. Sun, T. Ma, *Nat. Commun.,* 2024, **15**, 9576.

28 L. Zhang, X. Lu, J. Sun, C. Wang, P. Dong, *J. Mater. Chem. A,* 2024, **12**, 5392–5405.

29 X. Zhang, Z. Xiao, L. Jiao, H. Wu, Y. X. Tan, J. Lin, D. Yuan, Y. Wang, *Angew. Chem. Int. Ed. Engl.,* 2024, **63**, e202408697.
30 M. Y. Gao, C. C. Li, H. L. Tang, X. J. Sun, H. Dong and F. M. Zhang, *J. Mater. Chem. A*, 2019, **7**, 20193-20200.
31 C. C. Li, M. Y. Gao, X. J. Sun, H. L. Tang, H. Dong and F. M. Zhang, *Appl. Cata. B: Environ.*, 2020, **266**.
32 M. Luo, Q. Yang, W. Yang, J. Wang, F. He, K. Liu, H. Cao and H. Yan, *Small*, 2020, **16**, e2001100.
33 Y. H. Yao, J. Li, H. Zhang, H. L. Tang, L. Fang, G.-D. Niu, X.-J. Sun and F.-M. Zhang, *J. Mater. Chem. A*, 2020, **8**, 8949-8956.
34 Y. P. Zhang, H. L. Tang, H. Dong, M. Y. Gao, C. C. Li, X. J. Sun, J. Z. Wei, Y. Qu, Z. J. Li and F.-M. Zhang, *J. Mater. Chem. A*, 2020, **8**, 4334-4340.
35 H. Y. Zhang, Y. Yang, C. C. Li, H. L. Tang, F. M. Zhang, G. L. Zhang and H. Yan, *J. Mater. Chem. A*, 2021, **9**, 16743-16750.
36 T. Zhou, L. Wang, X. Huang, J. Unruangsri, H. Zhang, R. Wang, Q. Song, Q. Yang, W. Li, C. Wang, K. Takahashi, H. Xu and J. Guo, *Nat. Commun.*, 2021, **12**, 3934.
37 P. Dong, A. Zhang, T. Cheng, J. Pan, J. Song, L. Zhang, R. Guan, X. Xi and J. Zhang, *Chin. J. Catal.*, 2022, **43**, 2592-2605.
38 W. Han, L. H. Shao, X. J. Sun, Y. H. Liu, F. M. Zhang, Y. Wang, P. Y. Dong and G. L. Zhang, *Appl. Catal. B: Environ.*, 2022, **317**, 121710.
39 H. Yan, Y. H. Liu, Y. Yang, H. Y. Zhang, X. R. Liu, J. Z. Wei, L. L. Bai, Y. Wang and F. M. Zhang, *Chem. Eng. J.*, 2022, **431**, 133404.
40 H. Zhang, Z. Lin and J. Guo, *RSC Adv*, 2022, **12**, 14932-14938.
41 H. He, S. Chen, W. Bi, X. Wen, S. Sun, P. Zhang, R. Shen and X. Li, *Solar RRL*, 2023, **7**, DOI 10.1002/solr.202300532.
42 F. Ma, Q. Tang, S. Xi, G. Li, T. Chen, X. Ling, Y. Lyu, Y. Liu, X. Zhao, Y. Zhou and J. Wang, *Chin. J. Catal.*, 2023, **48**, 137-149.
43 R. Shen, G. Liang, L. Hao, P. Zhang and X. Li, *Adv. Mater.*, 2023, **35**, e2303649.
44 L. Hao, R. Shen, G. Liang, M. Kang, C. Huang, P. Zhang and X. Li, *Appl. Catal. B: Environ.*, 2024, **348**, 123837.
45 W. He, K. Kong, M. Wang, B. Dong, D. Yuan, K. P. Bryliakov and R. Wang, *Appl. Catal. B: Environ.*, 2024, **350**, 123916.
46 X. Huang and J. Guo, *Chin. J. Chem.*, 2024, **42**, 2621-2626.
47 S. Jiang, H. Niu, Q. Sun, R. Zhao, N. Li and Y. Cai, *J. Mater. Chem. A*, 2024, **12**, 11416-11423.
48 C. Li, B. Yang, R. Shi, N. Bao and Q. Dai, *Nano Today*, 2024, **56**, 102233.
49 W. Zhao, L. Luo, M. Cong, X. Liu, Z. Zhang, M. Bahri, B. Li, J. Yang, M. Yu, L. Liu, Y. Xia, N. D. Browning, W. H. Zhu, W. Zhang and A. I. Cooper, *Nat. Commun.*, 2024, **15**, 6482.
50 Z. Lin, X. Yu, Z. Zhao, N. Ding, C. Wang, K. Hu, Y. Zhu and J. Guo, *Nat. Commun.*, 2025, **16**, 1940.